SCIENTIFIC CULTURE
www.sci-cult.com

SCIENTIFIC CULTURE, Vol. 9, No. 2, (2023), pp. 1-28
Open Access. Online & Print

DOI: 10.5281/zenodo.7460006

REMARKS AND CAUTION ON FINDS OF KASTROULI MYCENAEAN SETTLEMENT (LOOFAH, CHARCOAL, BONE, WALL BURNT CLAY COATING, CERAMIC)

Liritzis, I.[1,2,3,4], Boyatzis, S.[5], Polymeris, G.S.[6], Panagopoulou, A.[7], Sideris, A.[8], Rapti, S[5]., Levy, T.[9, 10]

[1]Laboratory of Yellow River Cultural Heritage, Key Research Institute of Yellow River Civilization and Sustainable Development & Collaborative Innovation Center on Yellow River Civilization, Henan University, Kaifeng 475001, Minglun Road 85, China
[2]European Academy of Sciences & Arts, St. Peter-Bezirk 10, A-5020 Salzburg, Austria
[3]Edinburgh University, School of History, Classics and Archaeology, College of Arts, Humanities & Social Sciences, Dept of Archaeology, Edinburgh EH8 9AG, Scotland
[4]Rhodes University, Dept of Physics & Electronics, Makhanda (Grahamstown) 6140, Eastern Cape, South Africa
[5] Department of Conservation of Antiquities and Works of Art, University of West Attica, Agios Spyridonos Street, 12243, Egaleo, Greece
[6]Institute of Nanoscience and Nanotechnology, N.C.S.R. "Demokritos", 15310-Agia Paraskevi Attikis (Athens), Greece (g.polymeris@inn.demokritos.gr)
[7]Department of World Archaeology, Faculty of Archaeology, Leiden University, Einsteinweg 2, 2333 CC Leiden, The Netherlands
[8]Charles University, Institute of Classical Archaeology, Celetna 20, 1100 Praha 1, Prague, Czech Republic (thanos_sideris@hotmail.com)
[9]Center for Cyber-Archaeology and Sustainability, Qualcomm Institute, University of California, San Diego, La Jolla, CA 92093, USA (tlevy@ucsd.edu)
[10]Leon Recanati Institute for Maritime Studies, University of Haifa, Israel

Received: 22/03/2022
Accepted: 10/01/2023
Corresponding author: I. Liritzis (liritzis@henu.edu.cn; ioannis.liritzis@euro-acad.eu)

ABSTRACT

The excavated materials of the Late Helladic III settlement Kastrouli in Phokis, Greece has produced significant diverse information regarding chronology, human mobility, diet, characterization and provenance. The comingled burial of Tomb A and the finds from at least two buildings also contained some strange materials which properly analyzed offer a plea for caution. Moreover, they offer an opportunity to examine technological aspects, identification of species, dating and firing conditions.

The few materials investigated here by Optical microscopy (OM), SEM-EDS, FTIR and ^{14}C include some spongy-like fibers, an incised ceramic sherd, a burnt bone, burnt clay and four radiocarbon dates of charcoal and bone. It was found that the spongy material was ^{14}C dated to a modern loofah intruded in the tomb A; and the "decoration" in the grooves in the incised ceramic was remnants of the soil in which it was buried and not any possible incrustation or filling with unfired clay. The burnt animal bone analysis by FTIR provided a possible firing at ca 400-550 ^{o}C. The OM of the burnt clay has not produced any possible print textile. The radiocarbon dating of charcoal and one bone produced dates ca.13th c BCE, and the spans from 14thc BCE to late 12th C BCE is discussed in the light of wiggles during this period in the calibration curve.

KEYWORDS: Radiocarbon dating, Spectroscopy, Microscopy, excavation, Late Helladic, pottery, tomb, calibration, luminescence.

1. INTRODUCTION

Kastrouli is located in the Phokis area of central Greece, on the plateau of the peninsula of Desfina, southeast of Delphi, about 550 meters above sea level, and 4.7 kilometers east of the contemporary settlement of Desfina, between the shorelines of the Gulfs of Itea and Antikyra. The shortest distance from Kastrouli to the sea is towards Steno Bay, near Antikyra, on the Gulf of Corinth (5.1 km, Fig. 1), where Mastrokostas (1956, 24-25; also Sideris 2014, 35-36, figures. 3, 13-14) has already identified Mycenaean pottery and a potential fort.

The strategic location of Kastrouli between the gulfs of Kirrha and Antikyra allowed for control of the Mesokampos (mid plain) plateau as well as the entire peninsula of Desfina (Fig. 1). The two most important routes connecting Peloponnese with Central and Northern Greece have run from these gulfs since the Late Bronze Age. The famed Great Isthmus Corridor begins in Kirrha and traverses the highland neck between Mount Parnassus and Mount Ghiona, then another between Mount Oeta and Mount Kallidromo, eventually leading to the Spercheios valley (Kase et al. 1991). The second path, which is less popular due to its length, begins in Antikyra, detours through Daulis to Parnassus, and leads to Pylaea.

Despite its prominence in historical and mythological accounts, the ancient region of southern Phokis in central Greece has been approached mostly as a backdrop for more renowned neighbors (e.g., Delphi, Boeotia), the functions of which have been codified in surviving histories. Archaeological investigation has also been limited, resulting in southern Phokis remaining relatively untouched and unintegrated into the greater narratives of each of antiquity's key periods (Koh et al., 2020)

The southern part of Phokis has been historically "defined," but it has been mostly ignored, both in the Bronze Age and subsequent periods, relegated to relative dimness, and largely excluded from contributing more substantively to our broader understanding of Classical and Mediterranean antiquity. This necessitates an archaeological and scientific approach to bringing to light the rich past of southern Phokis, beginning with Kastrouli and expanding to coastal sites such as Steno, Antikyra, and Medeon, as a required supplement to any investigation (McInerney, 2011).

Thus, despite the harsh relief of the land and the unsettling presence of Parnassus in its center, Kastrouli was a part of a vast Late Bronze Age network of tiny forts and fortified towns that connected and effectively safeguarded the inhabitants of Phokis (Philippson & Kirsten 1951, 414-415; McInerney 1999, 303-306, 345-347, map 8). According to Tartaron (2013, 1-6), nothing is known regarding the locations and actual uses of Mycenaean anchorages and harbors. The local networks of marine contacts in the Mycenaean world are poorly understood, despite the fact that researchers know quite a bit about long-distance Late Bronze Age trade throughout the eastern Mediterranean. A suitable "open-air" land and marine environment is provided by the Gulf of Corinth, locations like Kastrouli, and the nearby coastal zones.

As recorded in Levy et al., (2018) "*It seems everything is debated in Mycenaean archaeology, including the notion of a "core area" of settlement. For this study, we assume that the Peloponnese and central Greece, which include Kastrouli and the Gulf of Corinth, are indeed part of the Mycenaean core area of settlement making this project a significant data source for examining the LBA issues noted above. The Kastrouli and Antikyra Bay coastlines were and still are tightly linked as a locus for economic and social intercourse making them an ideal setting for investigating a Mycenaean coastal world*".

The Kastrouli settlement has been excavated for three consecutive seasons (2016-2018) by an international team leaded by the University of the Aegean (up to 2020) and thereafter by the Ephoreia of Antiquities of Phokis[1]. Interdisciplinary specialists have revealed significant artifacts, tombs and buildings the material culture of diversified nature has been investigated by archaeometric techniques (Sideris 2022; Sideris et al., 2017; Sideris and Liritzis 2018; Levy et al., 2018; Koh et al., 2020; Liritzis 2021; 2022) (see papers in www.kastrouli.org).

Chronology of occupational phases, characterization and provenance of clay fabric, ceramic technology, ancient DNA of bones and bone diagenesis are a major publication output produced so far (Kontopoulos et al., 2019; Liritzis et al., 2020; Lazaridis et al., 2022).

The aim of the present investigation focuses on analyses of particular finds, including the type of fibers found in the Tomb A, some wall burnt clay coating found in close to the internal wall of a building 1, incised ceramics and reevaluate some charcoal radiocarbon dating (Polymeris et al., 2023). The results are discussed and compared with earlier published data of ages on bones by ^{14}C dating and ceramics and stone by surface luminescence dating.

[1] The initiator and managing director (Ioannis Liritzis, physical sciences-archaeometry) has undertaken a methodological approach based on interdisciplinarity, in collaboration with archaeology director (Athanasios Sideris) along with occasional co-PI directors (Tom Levy, UCSD and Andrew Koh, MIT, Kate Birney, Wesleyan Univ), and this collaboration has produced various publications.

2. METHODS AND INSTRUMENTATION

The present follow up work has been the outcome of a collaborative effort for measurements and instrumentation at respective laboratories.

SEM-EDX at West Attica University (UNIWA): Scanning Electron Microscope-SEM JEOL JSM–6510LV, on low pressure vacuum 20Pa, and 20kV accelerating voltage. Elemental analysis of the samples was carried out with Energy dispersive X–ray spectroscopy (EDS), with a JEOL JSM 6510LV SEM, on low pressure vacuum 25Pa, 20kV accelerating voltage. The instrument is equipped with an X–act Pentafet Precision detector (INCA analysis system, Oxford Instruments).

FTIR spectra of KBr-pressed samples were recorded in the University of West Attica (UniWA), Department of Conservation of Antiquities and Works of Art (CAWA) with a Perkin Elmer Spectrum GX FT-IR Spectrometer. In all cases, spectra were recorded in the range 4000-500 cm^{-1} with 4 cm^{-1} resolution. Attenuated total reflectance infrared (ATR-FTIR) spectra were recorded in NCSR Demokritos (Institute of Nanoscience and Nanotechnology), with a Nicolet 6700 FT-IR spectrometer (Thermo Scientific, Waltham, MA, United States) equipped with a Specac attenuated total reflectance (ATR) accessory using a diamond internal reflection element (refraction index 2.4).

Optical Microscopy at UNIWA: The observation and identification of the fibres was carried out on a LEICA DMLP, OLYMPUS Soft Imaging Solutions microscope, equipped with colour view camera (Soft Imaging System). Photos were taken with transmitted light and the use of polarizing filters in magnifications 10x, 20x, 40x.

NCSR Demokritos: Binocular polarising microscope, Leica DM2700P with the Leica MC190HD camera.

NCSR Demokritos: portable Energy dispersive X-ray fluorescence spectroscopy (EDXRF). Handheld portable Thermo Scientific™ Niton™ XL3t XRF Analyzer (pXRF) (Waltham, MA, USA) was used with a measurement time of 120 s under a standard atmosphere.

NCSR Demokritos: Polarizing and Scanning electron microscope (SEM-EDS) (FEI, Quanta Inspect D8334 SEM-EDS). The EDS was operating with a voltage of 25 kV, and spectra with a live time of 100 s were recorded in order to obtain the optimum excitation of the low-energy and low-concentration elements. Analytical totals, typically in the range of 95–99%, were normalized to 100%.

Radiocarbon dating: NCSR Demokritos and University of California, Irving (AMS) and one sample from Queen's University Belfast, following their analytical procedure quoted in various papers. At NCSR Demokritos each of approximate mass 6 grams, were collected and processed at the radiocarbon Unit of the Laboratory of Archaeometry, NCSR "Demokritos" (code DEM-), which uses the Gas Proportional Counting technique (GPC). This technique involves turning the sample into carbon dioxide (CO_2) gas and detecting the radioactivity through the beta particles that are released when the 14C atoms decay in cylindrical gas proportional counters (Maniatis 2013; Maniatis et al., 2016).

Due to their corresponding low mass, two charcoals were processed at the KECK Carbon Cycle AMS Facility, Earth System Science Department, in UC Irvine, USA (code UCIAMS-), which uses the Accelerator Mass Spectrometry (AMS) technique. A modified ABA procedure was applied, using 1N NaOH and 1N HCl at 75° C prior to combustion and graphitization. All ^{14}C ages were calibrated to calendar ages with the IntCal20 calibration curve (Reimer et al., 2020). Only DEM results have been corrected for isotopic fractionation according to the conventions of Stuiver and Polach (1997), with $\delta^{13}C$ values.

3. THE KASTROULI SETTING, SAMPLES AND SAMPLING

Fig.1 gives the geographical setting of Kastrouli and locations where the analyzed samples were taken from: bones from Tombs A and B, charcoals from Buildings 1 and 2, fibrous from Tomb and ceramics, mortar from Building 1, 2.

Table 1A gives a description of the analyzed samples and their reference codes along with images of the samples (Fig.2) and Table 1B the new radiocarbon dated samples.

(A)

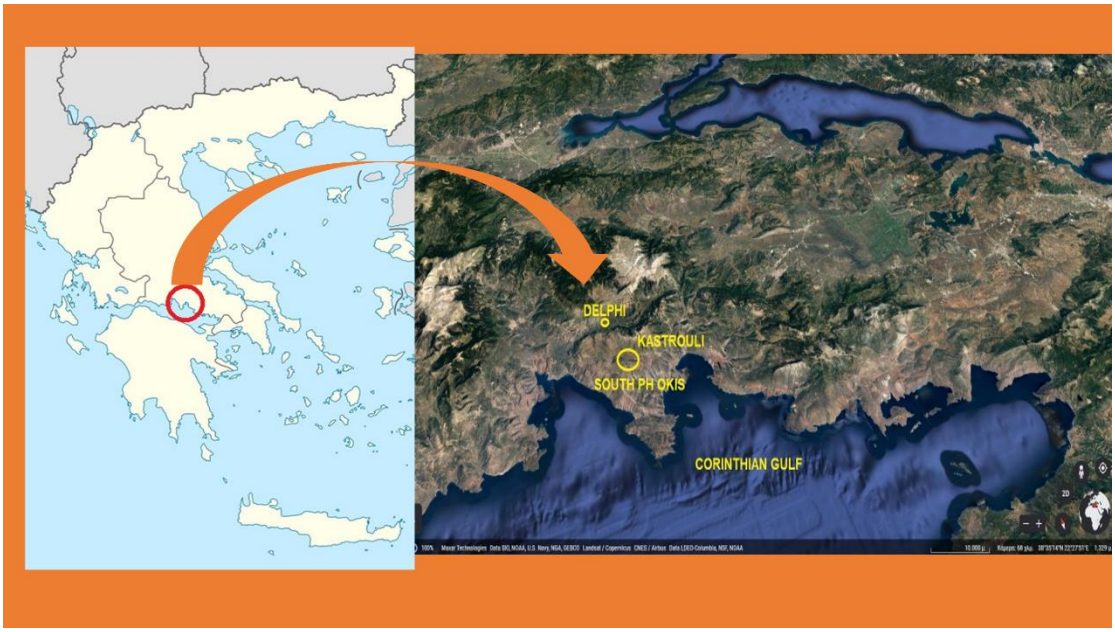

(B)

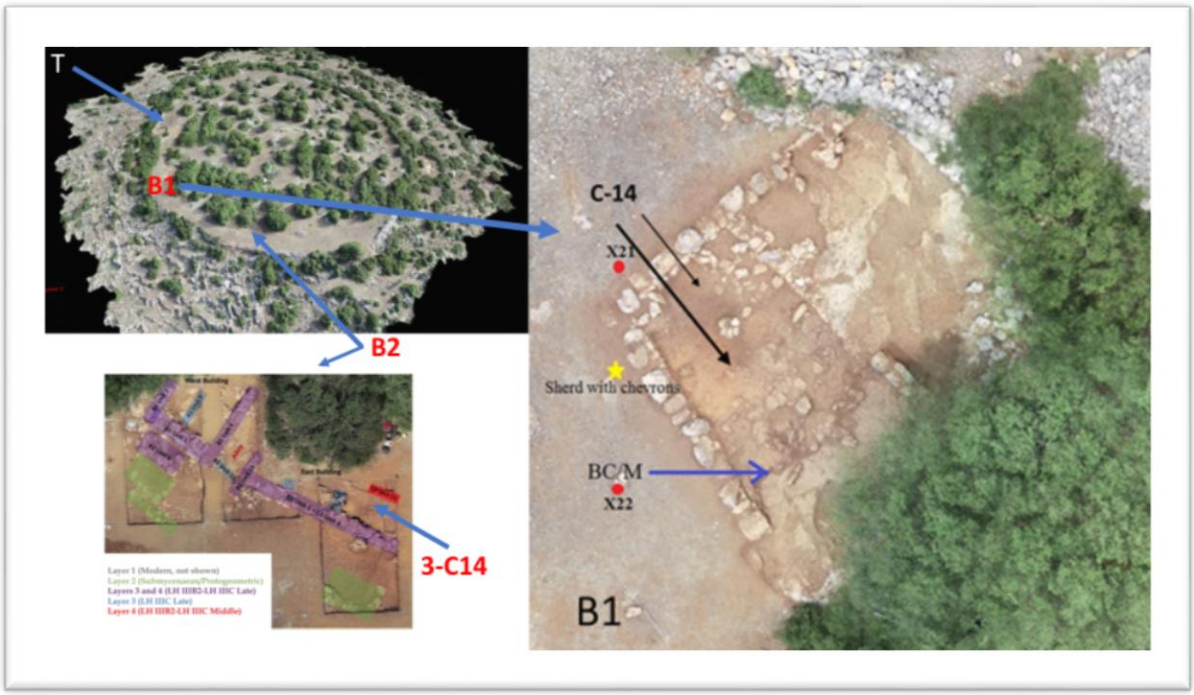

Fig. 1 A: The location of Kastrouli (yellow circle) in Phokis, B: The Kastrouli circular settlement with the tomb A (T) and the buildings B1 and B2 and the sampling positions in Buildings 1, 2. The C14 are for the two radiocarbon dating locations, the T is the tomb, BC/M the burnt clay/mortar (B and C taken by drone photographer Ian Roy, based on Koh et al., 2020; Sideris 2022).

The Table 1A gives the sample description and Table 1B the sampling locations for charcoal. The exact location is considered essential for any future researchers' revisit and re-analysis of finds of same context.

Table 1A. Sample code of samples analyzed corresponding to Fig.1 (T=tomb A). Code numbers are provided by the excavators in respective locations of the dig (Levy et al., 2018). Loci and artifacts are located by GPS and these points provided base control points for the total station/ArchField recording for the entire excavation to maintain consistency.

1.KASTROULI 2016_L.121_Sq.6/19_B20140_BC97483818_YELLOW FIBERS (T)	
2.KASTROULI 2016_L.121_Sq.6/19_B20134_YELLOW FIBERS (T)	
3.KASTROULI 2016_L.121_Sq.6/19_B20159_BC29785241_BURNED ANIMAL BONE (T)	

4.KASTROULI 2018_BUILDING 2_BURNT CLAY POSSIBLE PRINT TEXTILE FRAGMENT (BC/M)	
5.KASTROULI 25/7/2018_WALL CERAMIC BETWEEN X21-X22_OUTER SIDE_WEST OF THE SW WALL	
6.KASTROULI 07/20/2018 Building 2-C3_UNIT10_G10_BUILDING B_BURNT WOOD CHARCOAL (B2, 3-C14)	
7.KASTROULI 2016_TOMB A_L.121, Sq6/19_B20109_BC84352657_HUMAN RE-MAINS_BAG BARCODE37352902_BASKET94776397 (T)	

Table 1B The new analyzed samples by radiocarbon

Lab No	**Sample No/Context**
8. DEM – 2803	Building 1, (Fig 15 Sideris & Liritzis 2018) this was found north of the south/southwest exterior wall of the building in 2017. (B1, 2-C14)
9. DEM – 2733	Building 2, KAS-B2-2018, Charcoal 20/7/2018, C3 Unit 10, G10 (B2)
10. UCIAMS-253532	Building 2, KAS-B2-2018, charcoal 20/7/2018, C3, UNIT 10, PB#141, G10 (Koh et al., 2020). (B2)
11. UNIAMS-253533	KAS-B1-2017 Building 1 3.20m from west wall, 3.70 m from south, 20 cm depth (at the east) (Sideris and Liritzis 2018) (B1, 1-C14)
12. UCIAMS - 253541	KAS2-TA-2016 Human bone R. Femur (P). From Tomb A comingled burial, human bone, has 7%collagen from earlier data on bone diagenesis (Kontopoulos et al., 2019) (T)

1

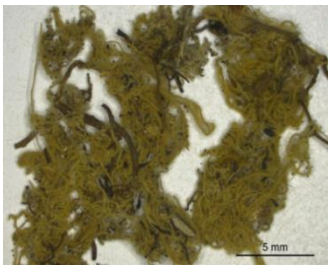

2

3

5

Building 1, mortar, interior southern wall

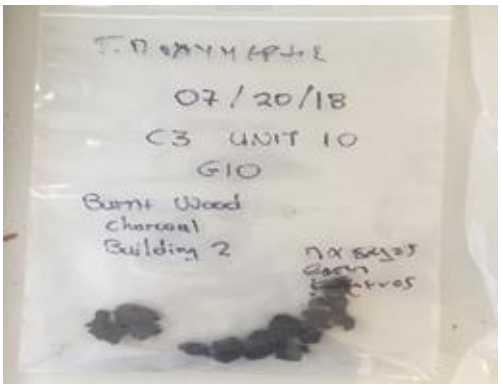

6

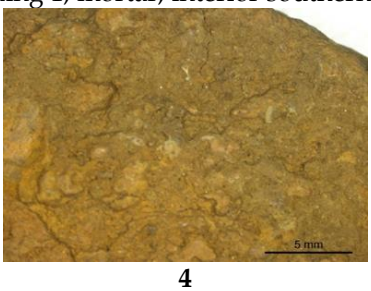

4

7

Building 2, 20/7/2018, C3 Unit 10, G10

Building 2, 2018, KAS-B2-2018, UCIAMS-253532

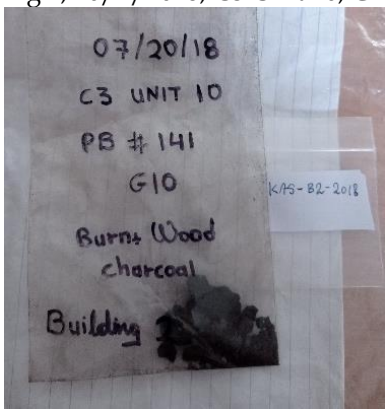

KAS-B2-2018, charcoal

KAS -B1-2017, Building 1

The 2 charcoals and 2 bones analysed

Figure 2. The organic and inorganic samples analyzed. Though a bit scattered and through a plastic bag this is intentionally added as such to ease future revisit of these samples and for documenting the relevant information of each one.

4. RESULTS

Fig 1 and 2 gives the location of samples in the excavated areas.

4.1 Burnt Clay-Mortar (Fig.2, No 4).

We gathered substantial burnt clay fragments from the south-eastern corner of Building 1 (or A), some of which had branch imprints on one side while others had smooth surfaces on both (Sideris 2022). Their clay has very few organic inclusions and is a rose-yellow color.

Their substantial thickness, ranging from 7 to 11 cm, appears to be prohibitive for the hypothetical covering of a roof constructed of branches. They are most likely wall coating pieces, while those with smooth

sides may have belonged to a storage structure in contact with the south-western wall, near the foundation of which they were discovered. Some remnants of this structure's base were discovered 2.30 m east of the building's western inner corner, at a depth of 40 cm.

It was most likely a rectangular construction with at least three smoothed and rounded corners. If it is not the lowest section of a storage facility, it could be the rim of a hearth, albeit the abundance of clay fragments, particularly those with both sides smooth, point to the former idea. A big sherd of pithos with an engraved linear design also originates from the same area.

A layer of burnt soil or pressed clay of intense orange to reddish color under a small layer of charcoal and ashes (1 cm thick) was found in the western section, a hue acquired normally when the clay is exposed to very high temperatures. After cleaning the visible north-eastern boundary of Building 1, it was discovered that a more recent retaining wall had been placed directly upon the building's original north-eastern wall, the lowest course of which is still visible in its original position.

Because the entire south-eastern side of the structure is now covered by big heaps of stones and thick vegetation of Palestine oak, it remained difficult to locate the wall that should connect the north-eastern to the south-western corners of the building (*Quercus calliprinus*). Building 1's tentative date based on ceramics shows that it was in use during the LH IIIC Early and probably Middle periods.

The fire destruction layer is more obvious in Building 2, where charcoal and ashes have been discovered, as well as a massive chunk of carbonized wood, presumably belonging to a roof beam. The burnt clays used in the wall coating (Fig. 2, No 4) are thinner (2-3 cm) than those used in Building 1. Deep and repetitive ploughing has severely altered and ruined the entire area south of the two buildings, making it difficult to correctly identify and link the few remaining structures today.

Fig. 3 gives some microscopic examination of the burnt clay/mortar which was examined for any imprint; but no obvious imprint are seen except of a type of plant roots in x6.3 scale taken at the NCSR Demokritos premises.

KASTROULI 2018_BUILDING B_BURNT CLAY	
	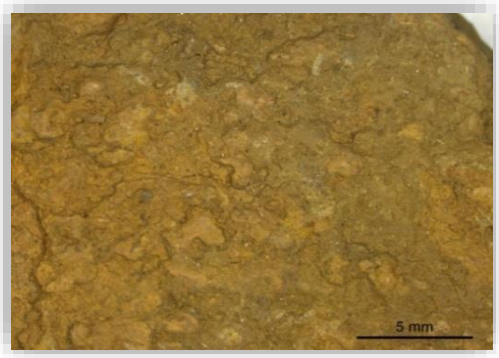
6.3x	6.3x
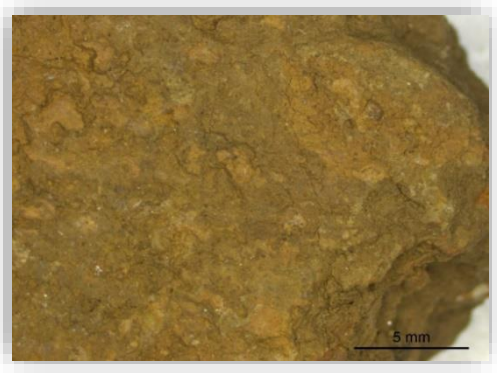	
6.3x	6.3x

	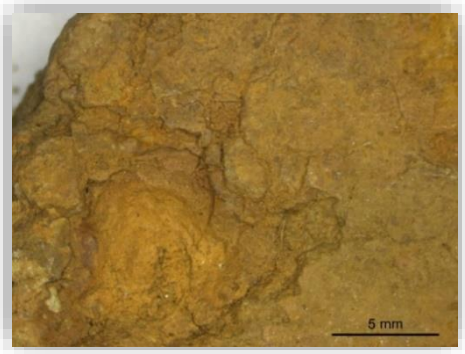
6.3x	6.3x
	
6.3x	10x
	
10x	6.3x back
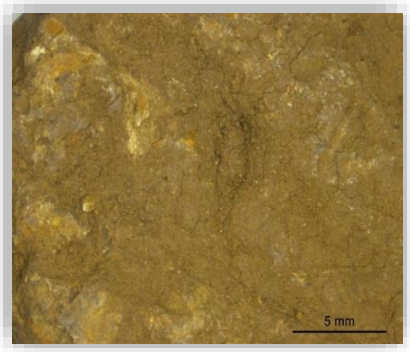	
6.3x back	

Figure 3. Microscopic images of the burnt clay/mortar from building 1

4.2 Burnt Bone

Locus 121 in the tomb A is characterized as a "dense accumulation of human bones (possible secondary burial) in southern chamber of tomb" (Sideris et al., 2017; Levy et al., 2018)

Amongst the successiveness of layers the Stratum III of loci 112 and 121 (see for loci in Levy et al., 2018), on the other hand, appear to be undisturbed, based on the density of reasonably intact human bones mixed with relatively big fragments of diagnostic ceramic sherds. Based on the disarticulation of the bones, L112 and L121, which reflect the same historical environment and are separated only for excavation purposes, appear to represent a multiple secondary burial.

Multiple burials in the tomb may have been gathered and concentrated in one area of the tomb to make room for further burials or activities in ancient times, according to grave goods and mixed bones of multiple people with no obvious orientation. Gold foil fragments, figurines, and intricately adorned ceramics have all been found, which suggests that at least one of the ancient burials may have held high-quality grave goods. Fig.2, No 3 shows the analyzed burnt bone and Fig.4A the microscopic analysis.

KASTROULI 2016_L.121_Sq.6/19_B20159_BC29785241_BURNED BONE

6.3x

6.3x

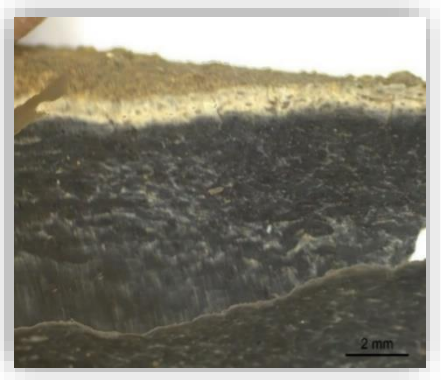

10x

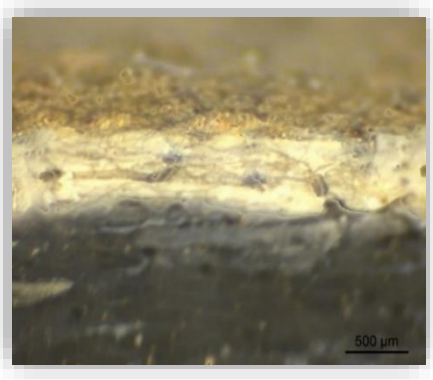

40x

(A)

(B)

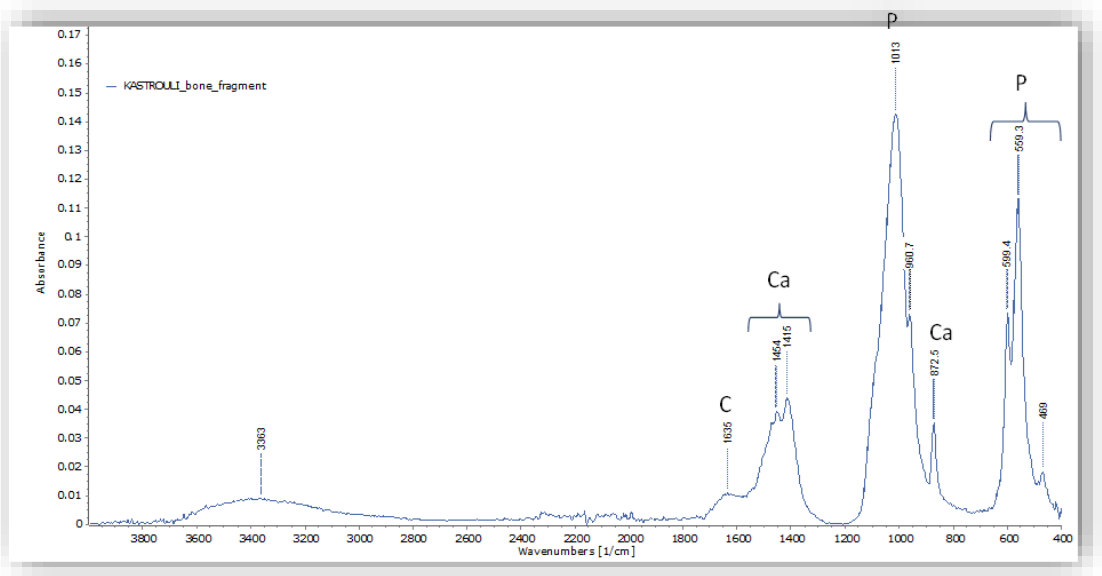

(C)

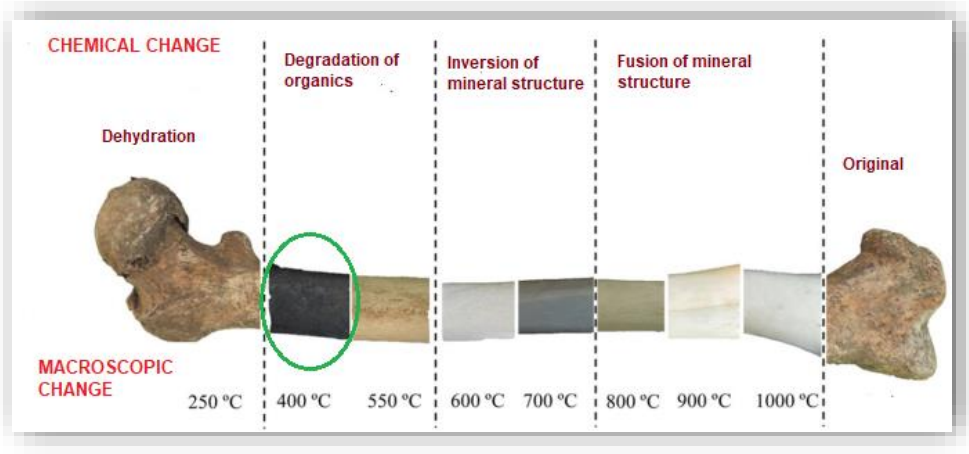

(D)

Figure 4: A) Optical Microscopy of the burned bone, B) a related burnt bone for macroscopic comparison (© Durham University + Teesside University; https://www.futurelearn.com/info/courses/forensic-archaeology-and-anthropology/0/steps/67912), C) Infrared spectrum of a powder sample taken from the burned bone fragment. C; collagen; Ca: carbonates; P: phosphates. Maxima at 1454 and 1415 cm^{-1} (carbonate stretching vibrations) are type A and type B carbonates, respectively and the one at 872 cm^{-1} (bending vibration) also appear as expected for typical bone material, D) representative color change in burnt bone at different temperatures, the green circle corresponds to our bone (based on Marques et al., 2018).

4.2.1 Optical Microscopy of the bone

According to the Optical Microscopy taken at the NCSR Demokritos premises., the cross section of this sample indicate that is burned bone due to the characteristic structure of bones (Ellingham et al., 2017). Bone is rigid body tissue consisting of cells embedded in an abundant hard intercellular material. However, as the two principal components of this material are collagen and calcium phosphate the pXRF analysis (taken at the NCSR Demokritos premises). proves that is a piece of bone. The main components of this sample are c. Ca 29% and P 10% following other elements in low concentration (Table 2).

Table 2 pXRF of the bone

Ca	28.89	**P**	9.82	**Si**	4.16	**Al**	1.55	**Fe**	0.70
K	0.30	**Ti**	0.12	**Pb**	0.07	**Mn**	0.06	**S**	0.10
Cl	0.10	**Cr**	0.01	**Sr**	0.01	**Zn**	0.01	**V**	0.01

Furthermore, the high balance c. 54% that is required to set the weight to 100% in Table 2 proved that it is due to the high amount of carbon (C) which cannot be detected with pXRF due to its detection limits.

The burnt bone from the comingled burial is absolutely irregular for this kind of funerary practice and it is highly improbable to be a human bone. On the contrary it may very well be an animal bone, which infiltrated the tomb during an ulterior funerary activity and, thus, it may be connected to a sacrifice. Indeed, the FTIR analysis below has confirmed this.

4.2.2 Infrared Spectroscopy of the bone

A powdered microsample taken from the burned bone fragment was analyzed with FTIR spectroscopy. As shown in the spectrum of Figure 4c, which consist of the organic and inorganic components, the protein part (representing collagen) appears significantly decreased as a result of the heat shock imposed on the material, and possibly, in combination with the diagenetic processes during the long burial period (Weiner, 2010; Kontopoulos et al., 2019; Boyatzis, 2022). On the other hand, the inorganic fraction (carbonated hydroxy-apatite, c-HAP) has survived, with the phosphate bands at 1013 cm^{-1} (phosphate stretching vibration) and the doublet at 600 and 559 cm^{-1} (bending vibration) being the most intense of the spectrum; besides, type A and type B carbonates with maxima at 1454 and 1415 cm^{-1} (carbonate stretching vibrations), and the one at 872 cm^{-1} (bending vibration) also appear as expected for typical bone material (Nielsen-Marsh and Hedges, 2000; Trueman et al., 2004; Weiner and Bar-Yosef, 1990). The relatively low amount of surviving collagen, in combination with the weak band at ~3360 cm^{-1}, suggest a possible heating range between 500 and 700 °C (Mamede et al., 2018; Marques et al., 2018). Judging also by the color (black), the exposure range could be limited to temperatures between 400-500°C (see Fig.4d). Infrared bands and assignments are listed in Table 4 below.

4.3 Ceramics incised

Fig.2 No 5 shows the piece of ceramic.

It is of interest that this ceramic sample from outside the west part of the SW wall of the Bulding 1 has a decorative technique with displacement and penetration.

The grooving consists in broad chevrons on a clay band slightly elevated from the rest of the vessel's surface (other similar fragments with such decoration have been found in the Tombs A and B and they all come presumably from large pithoi) (Sideris 2022, fig. 24, from Tomb B). The analysis of pXRF indicates the chemical composition of this ceramic fragment as well as the material with dark colour that has been intruded inside the decoration. This dark color material rather has several similar percentages of elements with the fired fabric, moreover the latter has been produced from local clays or with mixtures of local clays as earlier investigation has shown (Liritzis et al., 2020) (Table 3).

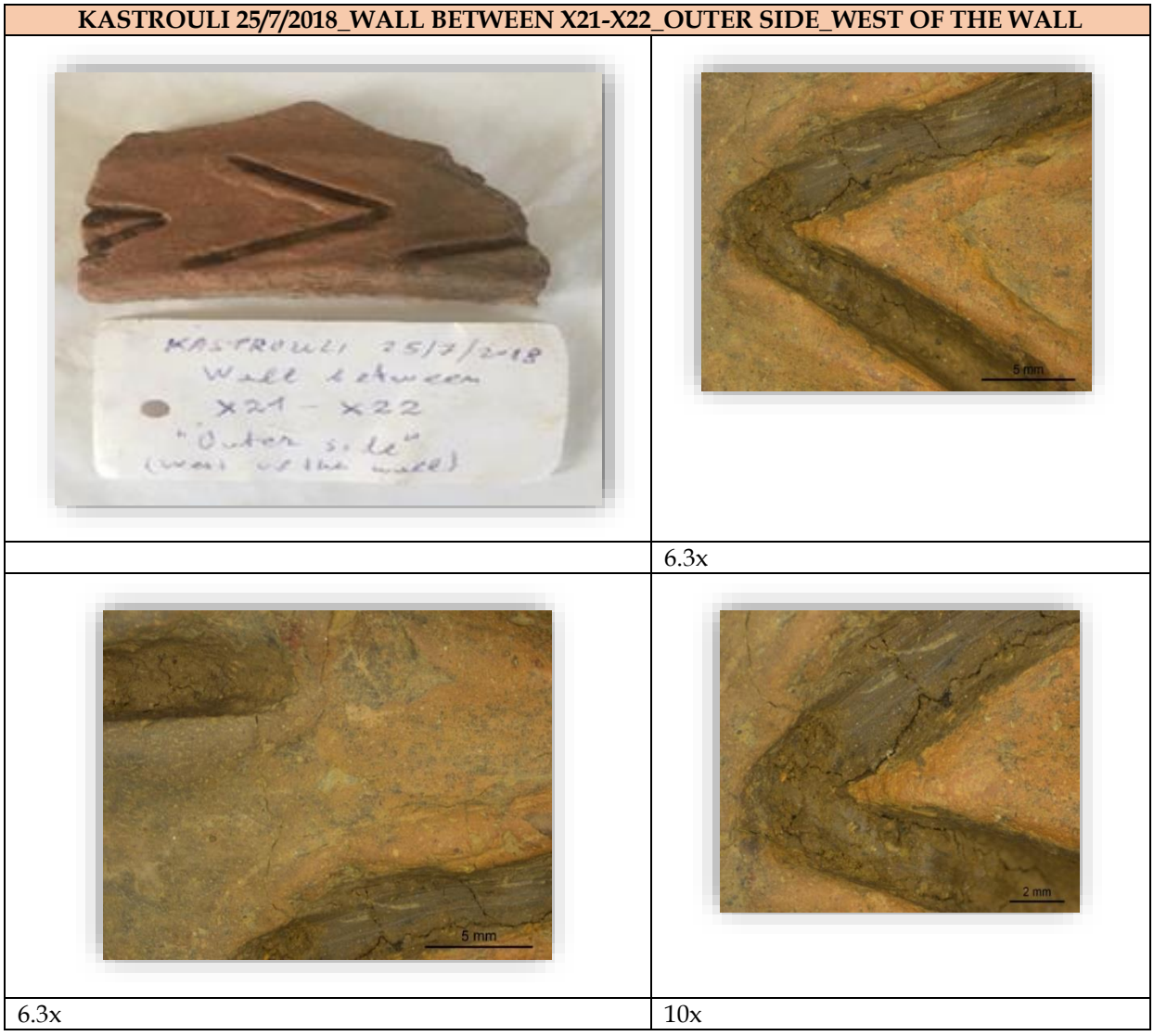

Figure 6. Optical Microscopy of the decoration of the under-study pottery fragment.

Table 3. Chemical elements in ppm by X-Ray Fluorescence Spectroscopy of the main fabric and the decoration taken at the NCSR Demokritos premises. Errors in measurements for most elements amount to ca.10-15%.

ELEMENTS	FABRIC	DECORATION	ELEMENTS	FABRIC	DECORATION
Ba	1008.7	737.5	**Fe**	32482	31310
Sb	28.3	34.4	**Mn**	994.7	939
Sn	22.8	21.6	**Cr**	106.5	164
Zr	186.5	178.8	**V**	100.8	104
Sr	85.9	69.7	**Ti**	3083	4669
Rb	102.5	117.7	**Ca**	88199.3	20514
As	10.6	8.3	**K**	13804.2	11193
Pb	30.2	28.6	**Th**	10.0	9.9
Zn	143.9	122.4	**Sc**	202.3	44
Cu	47.3	67.2	**Cs**	76.7	81
Ni	97.1	113.5	**Te**	93.1	116

Indeed, the "decoration" in the grooves is just remnants of the soil in which it was buried. Nevertheless, the obtained similar values in most elements may also reflect adherent surrounded soil on the ceramic's surface while the difference in calcium explains the origin of ceramic from the calcareous clay source, one

of the local clays, in contract to low calcium clay of the soil in the context.

The possible incrustation or filling with unfired clay is very unusual during this period of time and highly unpractical because the unfired clay when it dries, it shrinks and falls from the grooves mixed with surrounded sediment.

4.4 Organic fibrous material

The samples, brown-colored and with a fibrous texture, reminiscent of a weaved fabric, was found in the vicinity of human bones in Tomb A. Microscopic examinations, and elemental analysis had been carried out by the excavation team showing calcium (~30%), silicon (~27%), aluminum (~10%), iron (~10%), potassium, and phosphorus (variable). It has been exhaustively analyzed due to its obscure identification. Initially thought to be textile then plant and finally was proven to be loofah. Fig. 7 gives a first impression of the material of yellowish fibers mixed with little pieces of wooden branches. The images still sway hypothetical attribution to some kind of textile or plant.

Furthermore, based on the above, a hypothesis was made that the samples could be of textile fabric, possibly, either proteinaceous (for instance, wool, silk) or polysaccharidic (cotton, linen, etc.). For investigating the material in more detail, a methodology was applied as follows.

4.4.1 Optical and scanning electron microscopy of fibrous material

Examination of both fiber samples under the stereomicroscope (Figure 11a) and the Scanning Electron Microscope (SEM, Figures 11b and 11c), showed no structural connection to any type of weaved textile fabric; instead, images were reminiscent of a sponge-like natural organic material of biological origin. Besides, SEM images (see, for instance, Figure 11d) strengthened the above preliminary observation by being similar to sponges (collective term for marine organisms, members of the Porifera phylum) or other similarly-textured organisms, such as the plant loofah. Among the two, it seemed that the latter is most likely (Antcliffe et al., 2014; Voultsiadou 2007; Emery 2019).

Similar textures have been recorded elsewhere which was a confusing issue regarding preservation and if they are textile or some kind of plant (Gromer, 2016; Skals et al., 2018; Historic England 2016; Jayamani et al., 2014; Antcliffe et al., 2014 Thallemer 2020)[2].

KASTROULI 2016_L.121_Sq.6/19_B20134_YELLOW FIBROUS MATERIAL

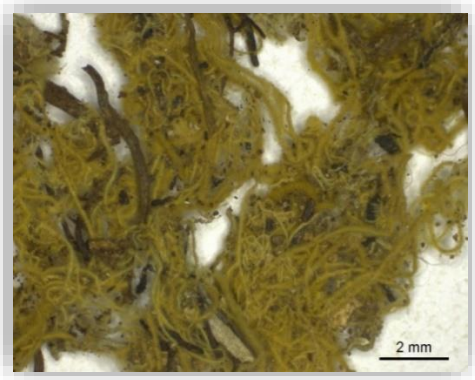

10x

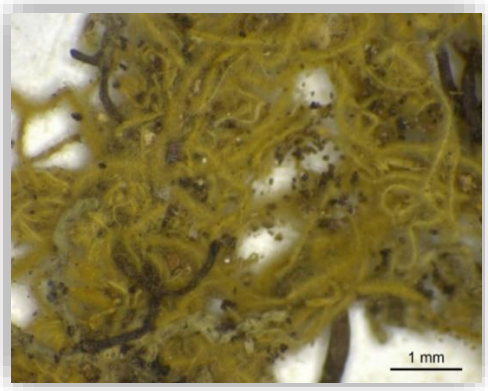

20x

[2] From correspondence with experts Prof Axel Thallemer and Dr Emilio Rodriguez-Alvarez, the possibility of being loofah was intriguing.

KASTROULI 2016_L.121_Sq.6/19_B20140_YELLOW FIBROUS MATERIAL

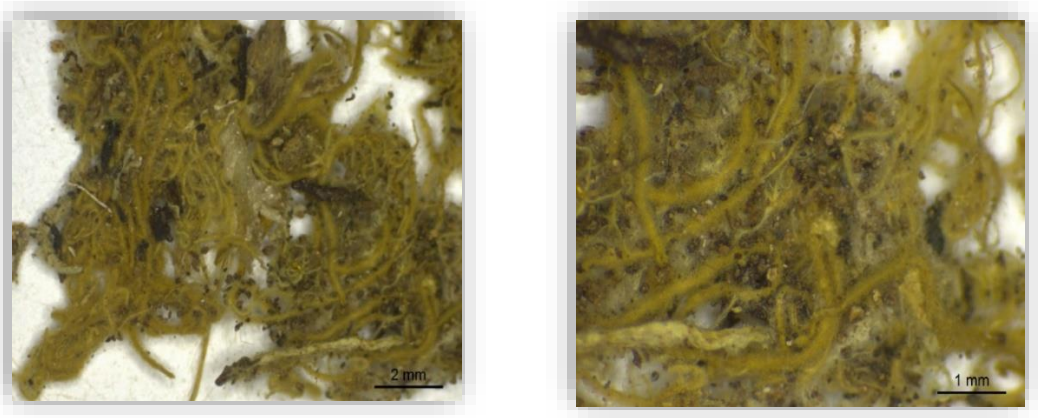

10x 20x

Figure 7: Microscopic magnifications of the yellow fibrous material. (taken at the NCSR Demokritos OM)

Fig.8 gives a better expansion of the fibres with SEM.

KASTROULI 2016_L.121_Sq.6/19_B20134_YELLOW FIBERS

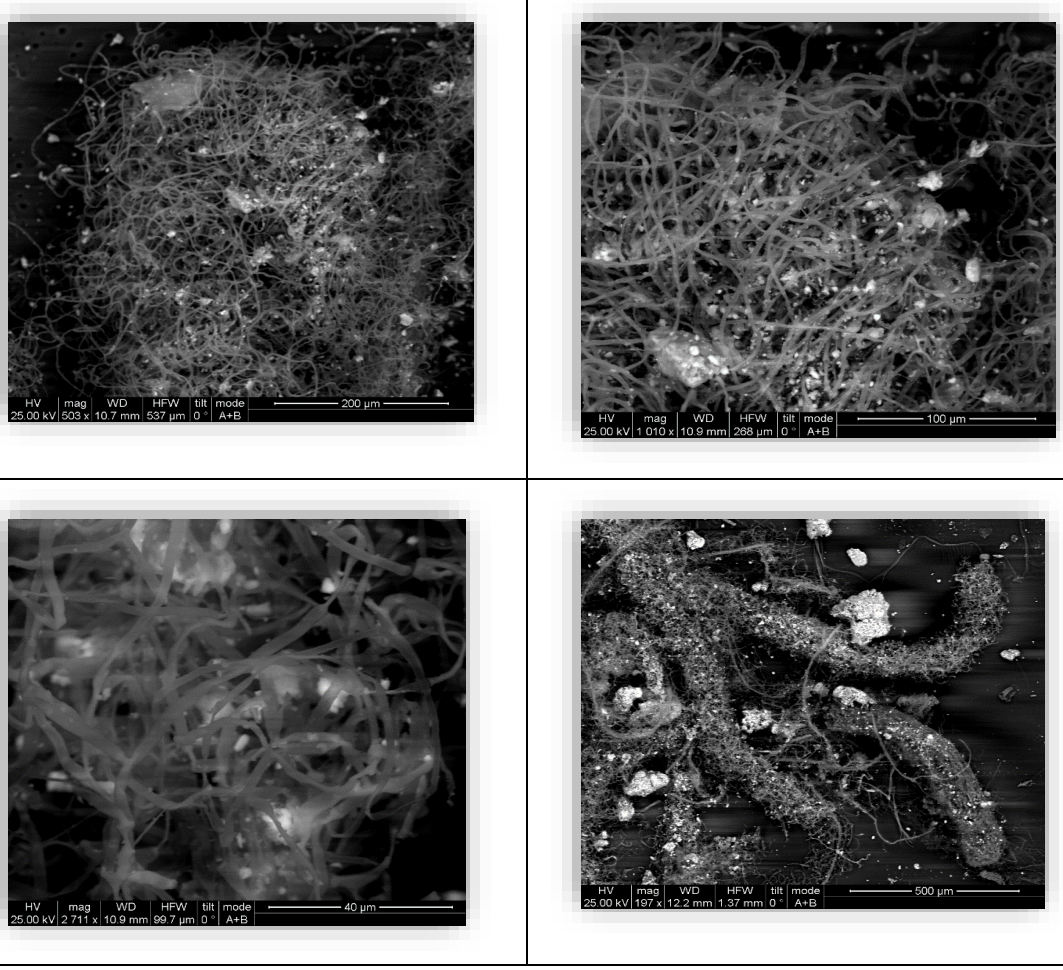

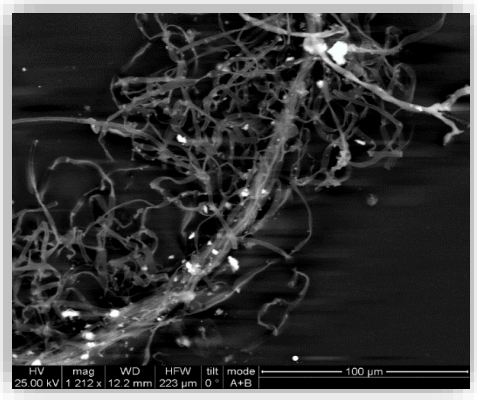

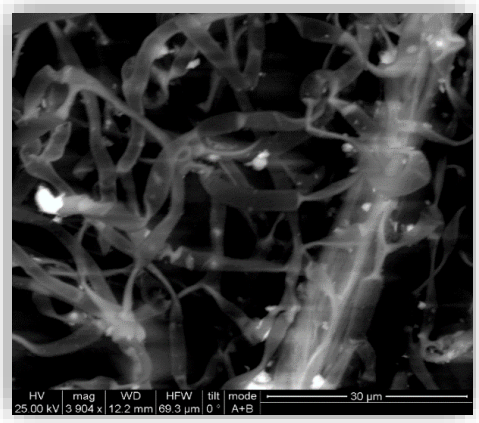

KASTROULI 2016_L.121_Sq.6/19_B20140_BC97483818_YELLOW FIBERS

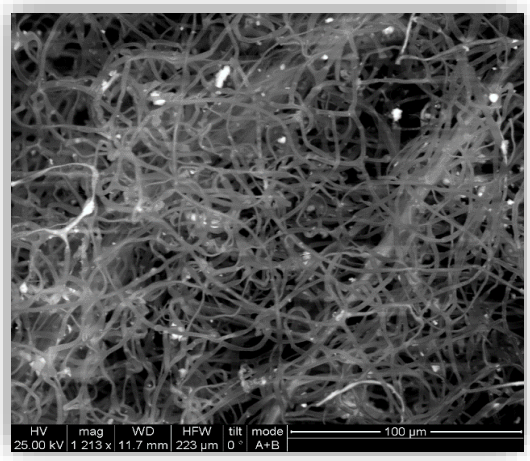

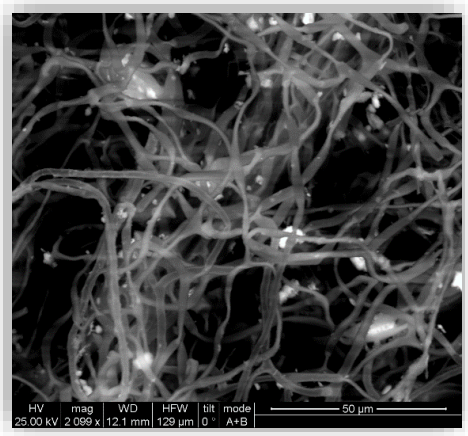

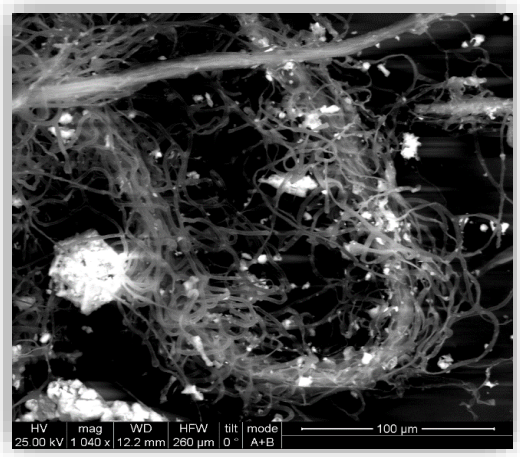

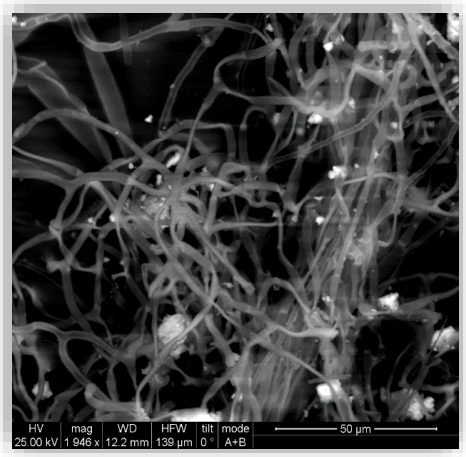

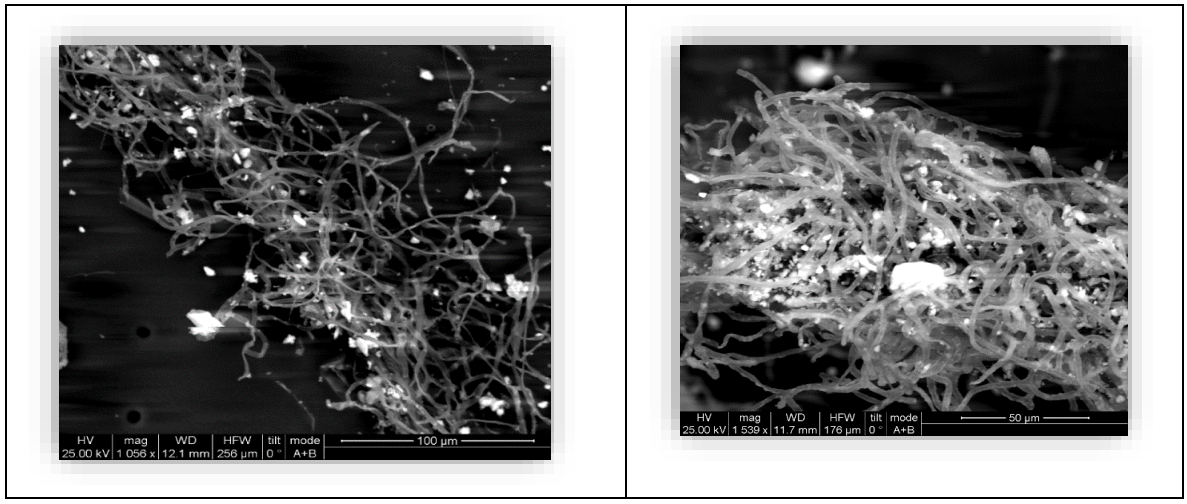

Figure 8: SEM images of the fibres (taken at the NCSR Demokritos SEM-EDX).

4.4.2. Fourier transform infrared (FTIR) spectroscopy of fibrous material

Infrared spectroscopy can provide information on the molecular bonding in organic and inorganic materials and can lead to the characterization of classes of compounds, such as biomolecules (polysaccharides, protein materials, fatty substances, etc.) Besides, provided that the spectra quality is adequately good, it can provide more specific detail about types in each of the above classes (Bitossi et al., 2005; Derrick et al., 1999; Griffiths and Haseth, 2007; Poliszuk and Ybarra, 2014; Steele, 2006).

For instance, infrared spectra of protein materials are quite characteristic due to their unique chemical character, specifically, concerning the peptide bond that connects amino acids forming the protein macromolecules (Bandekar, 1992; Barth, 2007; Barth and Zscherp, 2002; Lewis et al., 2013). Similarly, polysaccharide materials also give characteristic spectra, although their precise identification needs some extra attention as some of their bands fall within the same range as inorganic materials (e.g., silicates) (Brandenburg and Seydel, 2006; Kačuráková and Wilson, 2001; Liang and Marchessault, 1959; Wiercigroch et al., 2017). Consequently, protein materials can be identified and, based on their infrared spectra, further distinction can be made of whether they are made of collagen (such as bone, leather or parchment), keratin (such as hair/wool, nails or animal horns), and other materials such as silk; the above can be distinguished from polysaccharide materials, which, according to their infrared spectra can be further distinguished among starch, cellulose (for instance, cotton or linen), or other polysaccharides such as agar and various gums (Baker et al., 2014; Boyatzis, 2022).

Attenuated Total Reflection Infrared (or ATR-FTIR) analysis of the samples (without any workup) was carried to investigate their chemical nature. The spectra are shown in Fig. 9a and 9b, where bands at 3292, 1635, 1550, and 1250 cm^{-1} could be related to protein fiber such as wool. Other bands are also marked, such as those at 1030 cm^{-1} (the strongest in both spectra), 916, 800, 531, and 470 cm^{-1}, suggestive of silicate (earthen) material; this is in accordance with the elemental analysis results. For comparison reasons, a wool reference sample was also recorded (Figure 9c), where the characteristic amide A, B, I, II, and III bands (at 3276, 3070, 1632, 1515, and 1235 cm^{-1}, respectively) due to its proteinaceous character were detected. Comparison of the spectra suggest that spectra in Fig.9a and 9b are very similar, but most possibly they are not wool, as they have significant differences to the maxima of Fig.9c mainly in the absence of the 1030 cm^{-1} band in the latter, as well as the different maximum of the amide II band (at 1550-1554 cm^{-1} in Fig. 9a and 9b, as compared to 1515 cm^{-1} in Fig.9c).

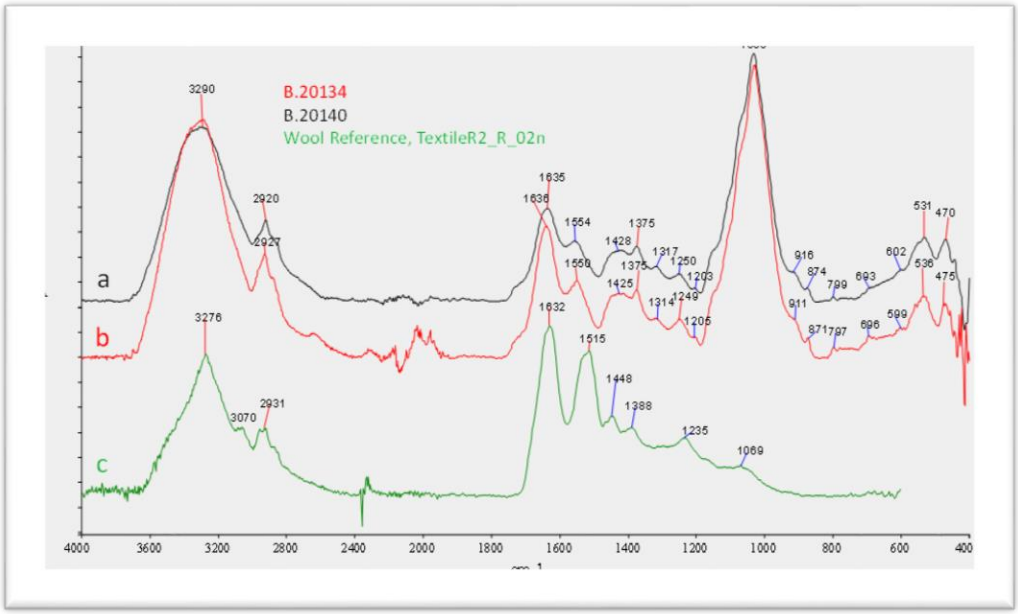

Figure 9. Spectra of unknown samples (a: B.20134, and b: B.20140) in comparison with protein textile wool, curve c).

To confirm the possibility of silicate materials and to obtain a clearer spectrum of the organic fraction, the geogenic sedimentary material was removed by rigorously shaking the samples, and its infrared spectrum was subsequently recorded, no processing with acids, solubles etc was applied (Fig.10b). The characteristic peaks confirm that the sedimentary material is clay (Boyatzis, 2022; Weiner, 2010). Subtracting spectrum 10b from the original spectrum (10a) results in spectrum 10c, which clearly shows the characteristic bands of lignocellulosic material with maxima at 1151, 1106, 1070, and 1028 cm^{-1}, along with maxima at 1635, 1558, and 1249 cm^{-1}, that can be related to the amide I, II, and II bands of a protein fraction (spectra shown in Fig. 10, assignments listed in Table 4).

Furthermore, infrared spectra of the archaeological samples were compared with those of a modern loofah sample (Fig. 10d), where close similarities were detected in both the lignocellulosic and the protein fractions (Mohamed et al., 2019); similarities were marked with dotted vertical lines across spectra of Fig.10.

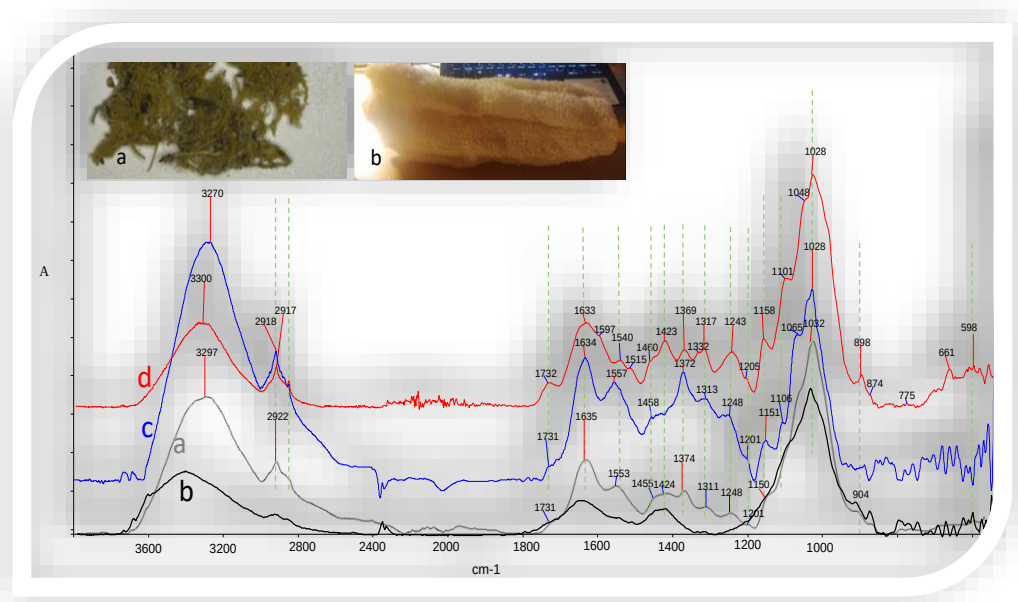

Figure 10: ATR-FTIR spectra of (a) sample B.20134; (b) detached geogenic sedimentary material; (c) sample B.2013 after subtraction of sedimentary material; and (d) modern loofah (reference sample). Vertical lines show the peak correspondence among samples.

Table 4. Infrared bands and assignments

Bone fragment		
Band maximum, cm^{-1}	**Assignment**	**Notes**
~3200(br)	vOH, vNH, vNH_2	Apatitic hydroxide Collagen
1664	vC=O with contributions from vC-N and δN-H; Amide I	Collagen
1542	vC-N with contributions from δ_{ip}N-H: Amide II	Collagen (obscure)
(1546), 1458	$v_3 CO_3^{2-}$	Carbonate, type A (hydroxide substitution) in c-HAP, doubly degenerate
(1465), 1415	$v_3 CO_3^{2-}$	Carbonate, type B (phosphate substitution) in c-HAP, doubly degenerate
1111(sh), (1070), 1031	$v_3 PO_4^{3-}$	Hydroxyapatite
980	$v_1 PO_4^{3-}$	Hydroxyapatite
872	$v_2 CO_3^{2-}$	Carbonate in c-HAP, both types
604, 562	$v_4 PO_4^{3-}$	Hydroxyapatite

Organic fibrous material				
Band maximum, cm^{-1}			**Assignment**	**Notes**
Archaeological sample B.20134(a)	**Archaeological sample B.20134(b)[1]**	**Reference loofah sample**		
3290			vO–H	Of polysacharide uits and crystalline water
2922	2917	2918	vC-H alkyl chains in most organics	
1731 (w)	1731 (w)	1731 (m)	vC=O (pectin esters)	Appears weakened in archaeological samples
1635 (m)	1634 (m)	1633 (m)	δH–O–H (water)	Crystalline water in polysaccharide molecular structure
-	-	1597 (sh)	vC=C (aromatic ring)	Lignin fraction; mostly removed in archaeological sample
1553 (m-w)	1557 (m)	1540 (m)	$vCOO^-$ (pectate esters)	Carboxylate salts in hemicelluloses/pectin fraction
-	-	1515 (sh)	vC=C (aromatic ring)	Lignin fraction; mostly removed in archaeological sample
1455	1458	1460	δCH_2 exocyclic (cellulose) $\delta_{as}CH_3$ lignin	
1424	1425	1423	δC–C–H + δ_{ip}C–O–H (cellulose) vC[Ar]=C[Ar] + δC–H (lignin)	Decreased in archaeological sample
1374	1372	1369	$\delta_s CH_3$	In hemicelluloses and lignin fraction
1248	1248	1243	vC–O (acetyl)	In hemicelluloses
1201 (w)	1201 (w)	1205 (w)	δC–C–H + δH–C[6]–O + vC–C + τCH_2 + δ_{ip}C–O–H	Typical in cellulosic materials

1160 (sh)	1151 (m)	1158 (m)	v_{as}C[1]–O–C + δC–C[1]–H (glycosidic linkage) δ_{ip}C[Ar]–H (guaiacyl lignin)	Cellulose: β(1→4) glycosidic linkage.
1100 (w, sh)	1106 (m)	1101 (m)	v_{as}C–O–C + vC–C	Cellulose
~1060 (sh)	1065 (sh)	1048 (sh)	vC–O + vC–C + δC–C–H	Cellulosic materials: cellulose and hemicelluloses
1030			v_{as}Si–O_b–Si	Overlapping peak due to silicates (clays); high amount due to earthen deposits.
1032	1028	1028	vC–O + δC–O–H	Typical of glucopyranose rings in cellulose
916 (sh)			δAl-OH	Silicates (clays)
(900)		898 (w)	vC δC–C[1]–H + vC–C	Cellulose: β(1→4) glycosidic linkage; its absence shows loss of material integrity.
		874 (w, sh)	$\delta_{oop}CO_3^{2-}$	Carbonates.
		661 (m-w)		δ_{oop}C–O–H + ring modes
		598 (m-w)		δ_{oop}C–O–H + ring modes

[1] Spectrum after subtracting geogenic depositions
v: stretch, *δ*: deformation (bend), ip: in-plane bend, oop: out-of-plane bend; s symmetric bend, as antisymmetric bend.

Table 5 gives the chemical elements by SEM-EDX for the two samples with major presence of Al, Si, P, Ca, K, Fe.

The encouraging result prompted us to date this unique sample. The loofah sample (few mgr) was AMS C-14 analyzed at Queen's University Belfast, by Gerard Barrett, $^{13}\delta C$ corrected and produced a radiocarbon fraction modern result of F14C = 1.0203 ± 0.0029 (UBA-46681). This means the sample is modern, i.e. post-dating 1950 AD. This suggests it is intrusive material.

Table 5. Analytical results by SEM-EDX of two samples with yellowish fibers found in L. 121, Tomb A, (codes B20134 and B20140).

Detected Elements	Kastrouli 2016 L.121_Sq.6/19_B20134 Yellow Fibers (in %)	Kastrouli 2016 L.121_Sq.6/19_B20140_BC97483818 Yellow Fibers (in %)
Mg	1.53	1.98
Al	10.37	8.88
Si	27.13	20.62
P	10.04	12.68
S	2.40	5.38
Cl	2.27	5.78
K	8.16	9.18
Ca	30.26	28.98
Fe	7.84	6.52
Total	100.00	100.00

5. THE NEW RADIOCARBON DATES FROM 4 CHARCOALS AND ONE BONE: A CRITICAL ASSESSMENT

Four charcoal samples are dated using radiocarbon: two charcoal samples collected and processed at the radiocarbon Unit of the Laboratory of Archaeometry, NCSR "Demokritos" (code DEM-), which uses the Gas Proportional Counting technique (GPC); and with two additional charcoal samples which due to their corresponding low mass, these were processed at the KECK Carbon Cycle AMS Facility, Earth System Science Department, in UC Irvine, USA (code UCIAMS), which uses the Accelerator Mass Spectrometry (AMS) technique (see, section 2 above, and Table 6) (see also Polymeris et al., 2023).

*TABLE 6.1. Charcoal context (*OxCal v.4.4.4 (Bronk-Ramsey 2021) with the latest 2020 data set was used for age calibration (Reimer et al, 2020). **DEM 2733 and UCIAMS-253532 similar context Building 2. Details of 95% probable ranges can be seen in Fig.13.*

Lab No	Sample No/Context	Material	Age ^{14}C (BP)	δ^{13}C (‰)	Cal.* (BC)	probability
DEM – 2803	Building 1, (Fig 15 Sideris & Liritzis 2018) this was found north of the south/southwest exterior wall of the building in 2017.	Charcoal	3058± 30	-23,35	1388 – 1271 1411 – 1226	(68,2%) (95,4%)
DEM – 2733**	Building 2, 20/7/2018, C3 Unit 10, G10	Charcoal wooden roof beam base	3103 ± 30	-26,16	1419 – 1306 1436 – 1281	(68,2%) (95,4%)
UCIAMS-253532	KAS-B2-2018 Building 2 20/7/2018, C3, UNIT 10, PB#141, G10 (Koh et al., 2020).	Burnt wood charcoal	3135 ± 15	-28,78	1436 – 1401 1447 – 1319	(68,3%) (95,4%)
UCIAMS-253533	KAS-B1-2017 Building 1 3.20m from west wall, 3.70 m from south, 20 cm depth (at the east) (Sideris and Liritzis 2018)	Burnt wood, Charcoal	2995 ± 15	-28.37	1265 – 1210 1368 – 1128	(68,3%) (95,4%)
UCIAMS - 253541	KAS2-TA-2016 From Tomb A comingled burial, human bone, has 7% collagen from earlier data on bone diagenesis (Kontopoulos et al., 2019)	Human Bone R.femur	3030±15	-	1372 – 1233 1382 – 1221	(68.3%) (95.4%)

Besides these 5 new dates, the analysis has included 7 additional radiocarbon ages from Lazaridis et al. (2022). Fig. 13 presents all unmodeled ages (^{14}C new, ^{14}C old and luminescence dating, see also Tables 6, 7, within the framework of the present study. These are 12 radiocarbon and 10 stimulated luminescence ages. All 5 new calculated radiocarbon range between 1447 and 1228 (calibrated) BC, falling well within the Late Helladic era, and specifically a later part within the LH III B 2 - LH III C Early[3] and the earlier part within LH II B - LH III B 1 (taking into account the periodization for Argolis, from where we also have similar Kylix and four-handled jars in Kastrouli) (see, Sideris 2022; Sideris et al., 2017, Fig.26). Moreover, one of the samples (lab. number UCIAMS – 2 53533) also extends to as late as 1128 cal. BC, right within the LH IIIC Middle. The relatively large errors that are associated with these ages imply that Kastrouli could have been active during the LH II B to LH III C Middle periods as well. Similar ages were also revealed for 5 radiocarbon ages as well as some among the stimulated luminescence ages from Liritzis et al. (2016; 2019; Lazaridis et al., 2022); all stimulated luminescence ages are presented in Liritzis et al., (2018), see also Polymeris et al., (2023). As Table 1 also reveals, two different charcoal samples of same spot in Building 2 were measured in two different radiocarbon laboratories. The results provide a validity check on the radiocarbon ages from the two charcoal samples (Mountjoy 1998; Deger-Jalkotzy & Bächle 2009; Wiener 2013; Vitale 2006). A combination of these two ages is presented in Fig. 14. Statistical analysis suggests that there is a probability of 81.2% that these samples are dated within 1436 and 1386 BC. However, one should remember that the radiocarbon date of the charcoal, which registers the destruction by fire (especially for beams), may be up to two generations younger than the construction time of the building.

[3] Approximate periodization (within 10-20 years) of Late Helladic III: LH IIIA1 1420–1370 BC, LH IIIA2 1390–1315 BC, LH IIIB1 1330–1230 BC, LH IIIB2 1230-1190 BC, LH IIIC (Early) 1190–1130 BC, LH IIIC (Middle)1130–1090 BC, LH IIIC (Late)1090–1060 BC, Sub-Mycenaean 1060-1000 BC, Proto-Geometric 1000–900 BC. (Knodell 2021; Vitale 2006; Mountjoy 1998)

At any rate the accuracy of a few decades of conventional ^{14}C dates in this time interval 3300-3000 BP is not attainable at all. Radiocarbon dates reported with a high accuracy (± 30 yrs) can be misleading. The main drawback for period of concern is the presence of problematic wiggles in the calibration curve, potential corrections needed to account for marine reservoir effects (the ^{14}C difference between terrestrial and marine derived carbon) and also the unconsidered freshwater reservoir correction of ^{14}C dates. Such reservoir corrections, if suitable evaluated, should need to be considered when dating bone (more specifically collagen in the bone). The dietary isotope ratio mass spectrometry (IRMS) of $\delta^{13}C$ and $\delta^{15}N$ should be examined to determine if dietary reservoir effects are present. Based on the assumption of linear mixing by linear interpolation the ratios for ^{13}C lie between the end-point values –12.5‰ (100% marine) and –21‰ (100% terrestrial) as described by Arneborg et al. (1999). In our dates of bones (Tables 6, 7) there may be a slight marine and dietary correction (^{13}C and ^{15}N data from Lazaridis et al., 2022).

We revisit the $\delta^{13}C$ and $\delta^{15}N$ isotopic data accompanying the ^{14}C dated samples which are measured by Elemental analysed isotope ratio mass spectrometry (EA-IRMS). In our data and the published ones from Kastrouli none of the $\delta^{13}C$ values are significantly depleted and the nitrogen values are consistent with isotopic values from Greece for C3 plants. The $\delta^{13}C$ values could indicate even a small marine contribution, and the elevated $\delta^{15}N$ values could also be caused by the consumption of high trophic-level food, or manured plant food, or other environmental/physiological parameters.

Table 7. C14 dates of bones from Tomb A and B (from Lazaridis et al., 2022; Polymeris et al., 2023; Liritzis et al., 2016)

Laboratory code	Sampling description	Age ^{14}C (BP)	$\delta^{15}N$ (‰)	$\delta^{13}C$ (‰)
PSUAMS – 6186 (KS-T2B)	Late Helladic Tomb A	3045 ± 25	10.31	-18.94
PSUAMS – 6187 (KS-T2C)	Late Helladic Tomb A	3015 ± 20	8.92	-18.90
PSUAMS – 6809 (KAS-4)	Late Helladic Tomb A	2975 ± 25	9.08	-19.45
PSUAMS – 6823 (KAS-10)	Late Helladic Tomb A	2990 ± 25	8.93	-18.90
PSUAMS – 7560 (KS-T1-4)	Late Helladic Tomb A	3030 ± 20	8.73	-19.10
PSUAMS – 7825	Tomb B Bag B10	2500 ± 20	10.1	-19.00
DHS – 6605 (Liritzis et al., 2016)	Tomb A/B?	2584 ± 26	_	-22.10
UCIAMS – 253541 (KAS2-TA-2016) (Polymeris et al., 2023)	Tomb A	3030 ± 15	9.13	-19.28

Along these lines it is worth recalling dietary uncertainties impact on reported dates and discuss this effect. Although atmospheric ^{14}C activities have changed over time, most analyses of regional groundwater assume that they were constant at 100 percent contemporary Carbon before to atmospheric bomb testing in the 1960s (pmC= percent modern carbon). This method produces conventional radiocarbon dates in years Before Present (BP), with 1950 AD equaling 0 years BP. Following input of ^{14}C-free C from calcite dissolution inside the aquifers, many approaches based on statistical corrections, major ion geochemistry, stable and radioactive isotopes exist to adjust for this. Local geogenic CO_2 and/or oxidation of ancient organic matter may also reduce ^{14}C activity.

Using ^{14}C to determine mean residence times (MRTs) presents additional challenges related to the input function of ^{14}C into the subsurface. Typically, it is believed that the ^{14}C activities of CO_2 in the unsaturated zone are in balance with the environment at the time of recharge. Though often much smaller than those of the atmosphere, ^{14}C activities of CO_2 in the unsaturated zone (^{14}Cuz) do occur.

For instance, Carmi et al. (2009) report that ^{14}Cuz activity in an Israeli coastal aquifer were roughly 54% higher than atmospheric levels. Similar low ^{14}Cuz activity that get less intense the deeper they are underground have been observed in other places. Despite the crucial part the unsaturated zone plays in regulating input ^{14}C activities, this topic is rarely mentioned, and there have been no attempts to address it. (Irvine et al., 2021; Carmi et al., 2009).

The significant of wiggles or plateaus in the calibration curve can be observed in the two dates for the bone (UCIAMS – 253541 KAS2-TA-2016) 3030 BP and charcoal (UCIAMS – 253533 KAS-B1-2017) 2995 BP, within 35 years of difference in radiocarbon years but following calibration the probability distributions of the age ranges are significant (Fig. 13). For the reasons listed above, the calibrated age ranges should be treated with caution as they may incorporate issues due to reservoir effects and are also subject to large uncertainties due to the region of the calibration curve they are derived from.

Last but not least we do not know what part of the trunk the charcoal which derives from the base of a

beam comes from. Necessary maintenance in the houses involves replacement of wooden beams in a period of two generations (ca 60 years). Such uncertainty is plausible, but does not change much our time range and interpretation.

All these sources of error induce a respective error in the final corrected radiocarbon age.

Hence due to the abovementioned restrictions, rarely discussed in published results, the interval of approx. 2 centuries uncertainties in the 95% confidence should be considered with caution in the discussion for the determination of narrow error bars desired by archaeologists. The above discussion has emerged in relation to the archaeological evidence (Sideris et al., 2017; Levy et al., 2018; Sideris 2022). The 12th c BC destruction at Kastrouli coincides with the recognized fall of Mycenaean civilization and Bronze age in SE Mediterranean (Cline 2014).

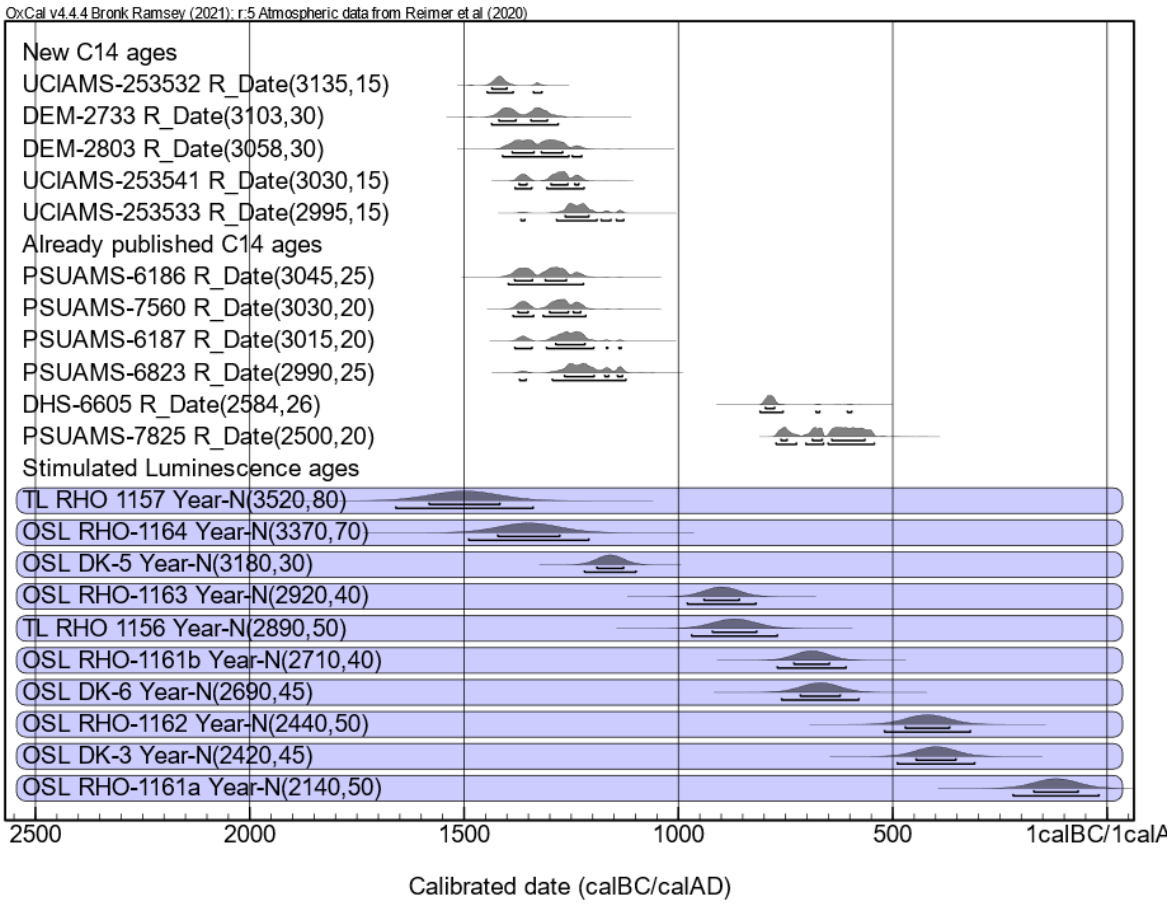

Figure 13. Unmodelled radiocarbon ages for all charcoal and bone samples (present and from Lazaridis et al., 2022), with the OSL ages of the pottery and stone samples from Liritzis et al., 2016, 2018) (in blue marking) are also presented for the sake of comparison. (NB: Regarding the PSUAMS – 7825 and DHS-6605 bones assigned to Tomb A and B are later period reuse of the tombs. In general, both are questionable regarding context as it seems to be a mismatch since Tombs A and B are definitely Mycenaean (and in Tomb B a figurine Φ was found among its structure - it cannot have been intruded though, plus the fact that the osteological examination showed that there was only one dead person).

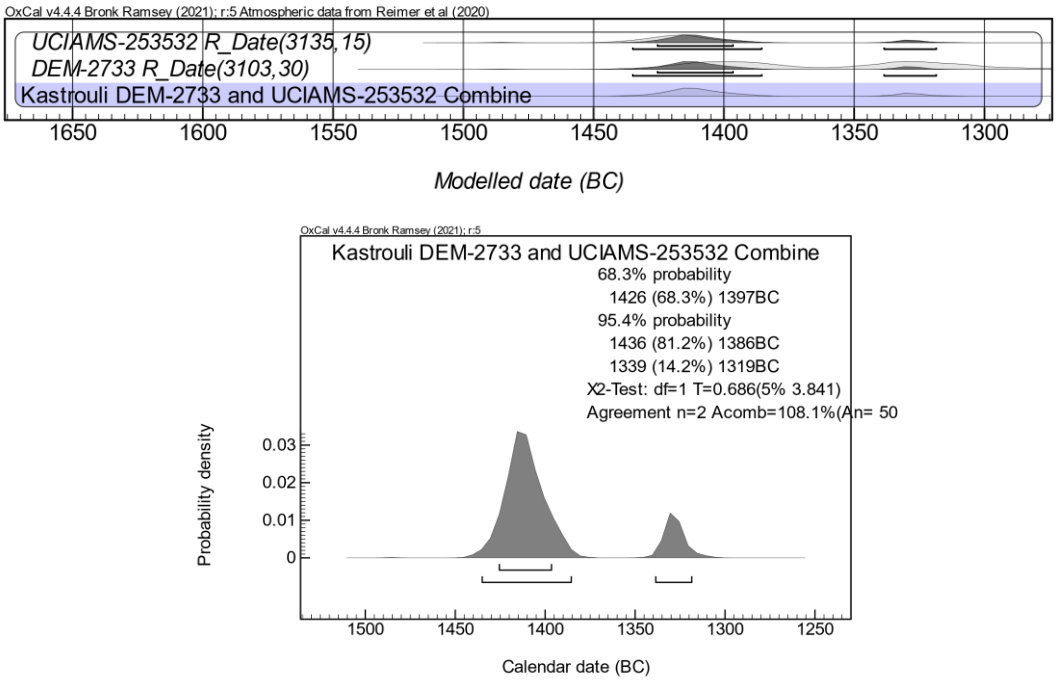

Figure 14. Modelled radiocarbon ages for the two samples with lab codes DEM 2733 and UCIAMS-253532 from Building 2.

6. DISCUSSION & CONCLUSION

The characterization and dating of some finds applying complementary techniques helps to decipher some puzzled cases. The prompt attribution of an artifact without meticulous investigation leads to questionable results.

The incised ceramic, the "modern" loofah, and more dates to understand the occupational period of the settlement strengthens the resulted investigation and recommends a plea for patience before jumping into unsupported conclusion. Calibrated radiocarbon dates should be treated with particular caution in particular considering the attached narrow errors from the measurement, in the presence of wiggles in the calibration curve and the need for reservoir correction. In the time intervals with a wiggly character a reasonable accuracy lies within at least two centuries span where age ranges expand with different probability (see Fig.13). The loofah presence is a unique find yet the identification and dating produced a modern result which suggested intrusive material.

The incised ceramic with grooves proved being remnants of the soil in which it was buried. The initial suspicion of a possible incrustation or filling with unfired clay is unattainable and very unusual during this period of time and highly unpractical because the unfired clay when it dries, it shrinks and falls from the grooves.

The decorative method with displacement and penetration also includes incision, impression, fluting, and dotted decoration because each of these decoration methods required pressure to be applied to the surface in order to remove or displace clay and produce the desired motif. The vessel's entire surface or only a part of it may be covered in any of the decorative motifs mentioned above (Rice 1987, 144; Rye 1981, 92). The most common way to use impressed decoration was to apply pressure to wet surfaces. The surface was impressed using a variety of tools including bones, reeds, sticks, shells, and sticks (Rice 1987, 144-5).

Regarding a bone fragment from Tomb A the Optical Microscopy indicated that it is burned bone compared to the characteristic structure of bones and from pXRF analysis.

The question of possible imprints as a type of plant roots in some burnt clay/mortar by microscopic examination did not reveal any obvious remains.

Overall, the Kastrouli settlement have opened a new chapter of peripheral world during the Late Mycenaean era. Dozens of articles have documented various aspects of life of southern Phokis region during the Late Mycenaean period and its termination coincides with the SE Mediterranean regional destructions and fall of great empires. The two looted tombs have destroyed much anticipated evidence especially their possible reuse. Reuse in archaic times is not entirely improbable, but extremely rare. Many times, in later times in antiquity open old Mycenaean tombs and make offerings (Medeon, Delphi) but not new burials. That is, the dead are treated as heroes (heroon, heroic cult). Hence the caveat about these

two tombs until new evidence in the future Moreover, it would be strange if two graves side by side were reused in Archaic times and all that was left was one bone in each, and not a trace of Archaic grave offerings. Anyway, reuse should be viewed with caution, though the settlement has been reused as surface finds and archaeometric dating has revealed. Further ongoing analytical results may shed light into the dietary mode and environmental landscape ecosystem.

Authors Contribution: Conceptualization, I.L.; methodology, I.L., G.S.P., A.B., A.P; software, G.S.P., A.B., A.P., I.L; validation, G.S.P., A.B., A.P.; formal analysis, G.S.P., A.P; investigation, I.L., A.S., G.S.P., A.B., A.M., T.L.; resources, A.P., A.B..; data curation, I.L., G.S.P., A.B., A.P.; writing—original draft preparation, I.L.; writing—review and editing, I.L., A.S., A.P., T.L; visualization, A.P., A.B., G.S.P.; supervision, I.L., A.S., T.L; project administration, I.L.; funding acquisition, T.L. All authors have read and agreed to the published version of the manuscript.

ACKNOWLEDGEMENTS

We thank the Ephoreia of Antiquities of Phokis and the Ministry of Culture & Sports for granting permission to analyze bone, stone, ceramics and charcoal remains. We thank Prof. A. Sideris the director of 2016-20 archaeological excavation, for his contribution in the discussion of dates as reported in previous publications. G.S. Polymeris acknowledges the valuable instructions received by Dr. Yannis Maniatis as well as Mrs Marigo Kyriazi for sample handling. T.E. Levy is grateful for having held the Norma Kershaw Chair in the Archaeology of Ancient Israel and Neighboring Lands at UC San Diego that supported this project. We also thank Dr. Fotis Katsaros, Senior Researcher in NCSR Democritos, for recording original FTIR spectra of samples. I. Liritzis is thankful to John Southon (University of California, Irvine); Benjamin Fuller (Oxford University), Bente Philippsen (Norwegian University of Science and Technology), Brendan J. Culleton (Penn State University) for valuable discussions on the radiocarbon and isotopic data; and to both Prof Axel Thallemer (Hong Kong University of Science & Technology) and Dr Emilio Rodriguez-Alvarez, (Universidade de Santiago de Compostela) for useful correspondence on sponges and loofah. We are thankful to Dr Gerard Barrett (School of Natural and Built Environment, Queen's University Belfast, United Kingdom) for dating the loofah sample and for thorough and critical comments on the drafted article. IL is grateful to the support of Sino-Hellenic academic project (www.huaxiahellas.com) by the Henan University, Laboratory of Yellow River Cultural Heritage, Key Research Institute of Yellow River Civilization and Sustainable Development & Collaborative Innovation Centre on Yellow River Civilization, Kaifeng, China. ^{14}C dates have been covered by Tom Levy grant.

REFERENCES

Antcliffe, J.B., Callow, R.H.T., and Brasier, M.D (2014) Giving the early fossil record of sponges a squeeze. *Biological Reviews* doi: 10.1111/brv.12090

Arneborg J, Heinemeier J, Lynnerup N, Nielsen HL, Rud N, Sveinbjörnsdóttir Á.E. 1999. Change of diet of the Greenland Vikings determined from stable carbon isotope analysis and 14C dating of their bones. *Radiocarbon* 41(2):157–68

Antcliffe,J.B., Richard H. T. Callow and Martin D. Brasier (2014) Giving the early fossil record of sponges a squeeze, *Biol. Rev*., pp. 1-33,, doi: 10.1111/brv.12090.

Bronk Ramsey C. (2021). *OxCal v. 4.4.4 [software*]. URL: https://c14.arch.ox.ac.uk/oxcal.html

Baker, M.J., Trevisan, J., Bassan, P., Bhargava, R., Butler, H.J., Dorling, K.M., Fielden, P.R., Fogarty, S.W., Fullwood, N.J., Heys, K. a, Hughes, C., Lasch, P., Martin-Hirsch, P.L., Obinaju, B., Sockalingum, G.D., Sulé-Suso, J., Strong, R.J., Walsh, M.J., Wood, B.R., Gardner, P., Martin, F.L., (2014). Using Fourier transform IR spectroscopy to analyze biological materials. *Nat. Protoc.* 9, 1771–91. https://doi.org/10.1038/nprot.2014.110

Baldinger, T., Moosbauer, J. and Sixta, H. (2000) Supermolecular structure of cellulosic materials by fourier transform infrared spectroscopy (ft-ir) calibrated by waxs and 13 C NMR, *Lenzing Berichte,* 79, pp. 15–17.

Bandekar, J., (1992). Amide modes and protein conformation. *Biochim. Biophys. Acta - Protein Struct. Mol. Enzymol*. 1120, 123–143. https://doi.org/10.1016/0167-4838(92)90261-B

Bandekar, J., and Krimm, S., 1979, Vibrational analysis of peptides, polypeptides, and proteins: Characteristic amide bands of β-turns, *Proc. Natl. Acad. Sci*. USA 76: 774–777.

Barth, A., (2007). Infrared spectroscopy of proteins. *Biochim. Biophys. Acta - Bioenerg*. 1767, 1073–1101. https://doi.org/10.1016/j.bbabio.2007.06.004

Barth, A., Zscherp, C., (2002). What vibrations tell us about proteins. *Q. Rev. Biophys*. 35, 369–430. https://doi.org/10.1017/S0033583502003815

Bitossi, G., Giorgi, R., Mauro, M., Salvadori, B., Dei, L., (2005). Spectroscopic Techniques in Cultural Heritage Conservation: A Survey. *Appl. Spectrosc*. Rev. 40, 187–228. https://doi.org/10.1081/ASR-200054370

Boyatzis, S.C., (2022). *Materials in Art and Archaeology through Their Infrared Spectra.* Nova Science Publishers, New York. https://doi.org/10.52305/SEYX8054

Brandenburg, K., Seydel, U., (2006). Vibrational Spectroscopy of Carbohydrates and Glycoconjugates, in: Chalmers, J.M. (Ed.), *Handbook of Vibrational Spectroscopy*. John Wiley & Sons, Ltd, Chichester, UK. https://doi.org/10.1002/0470027320.s8205.

Carmi, I., Kronfeld, J., Yechieli, Y., Yakir, D., Boaretto, E., Stiller, M.: (2009) Carbon isotopes in pore water of the unsaturated zone and their relevance for initial 14C activity in groundwater in the coastal aquifer of Israel. *Chem. Geol*. 268, 189-196, doi:10.1016/j.chemgeo.2009.08.010.

Cline, E.H (2014) *1177 B.C.: The Year Civilization Collapsed*, Princeton, Princeton University Press.

Casu, B. and Reggiani, M. (1964) 'Infrared spectra of amylose and its oligomers', *Journal of Polymer Science Part C: Polymer Symposia*, 7, pp. 171–185. doi: 10.1002/polc.5070070113.

Deger-Jalkotzy, S, Bächle A.E, eds. (2009) LH III C Chronology and Synchronisms III. LH III C Late and the transition to the Early Iron Age. *Proceedings of the international workshop held at the Austrian Academy of Sciences at Vienna*, February 23rd and 24th, 2007. Vienna.

Derrick, M.R., Stulik, D., Landry, J.M., 1999. *Infrared Spectroscopy in Conservation Science*. Getty Conservation Institute., Los Angeles. https://doi.org/10.1017/CBO9781107415324.004.

Ellingham, S.T.D; Tim J. U. Thompson, and Meez Islam, (2017) Scanning Electron Microscopy–Energy Dispersive X-Ray (SEM/EDX): A Rapid Diagnostic Tool to Aid the Identification of Burnt Bone and Contested Cremains, *J Forensic Sci*, 2017 doi: 10.1111/1556-4029.13541).

Emery E (ed) (2019) The global life of sponges, *Proceedings of the International Sponges Conference* [School of Oriental and African Studies], Island of Hydra, Greece, 19-20 May 2018, RN Books of London.

Gromer.K (2016) The art of prehistoric textile making. Natural History Museum Vienna.

Griffiths, P.R., Haseth, J.A., (2007). *Fourier transform infrared spectrometry*, 2nd ed. Wiley-Interscience, Hoboken, New Jersey. https://doi.org/10.1002/047010631X

Historic England 2016 Preserving Archaeological Remains HistoricEngland.org.uk/advice/technical-advice/archaeological-science/preservation-in-situ/

Irvine D.J, et al., (2021), Depth to water table correction for initial carbon-14 activities in groundwater mean residence time estimation. *Hydrology and Earth System Sciences, Discussions*, 1-17, https://doi.org/10.5194/hess-2021-276

Jin, X. et al. (2017) Determination of hemicellulose, cellulose and lignin content using visible and near infrared spectroscopy in Miscanthus sinensis, *Bioresource Technology.* 241, pp. 603–609. doi: 10.1016/j.biortech.2017.05.047.

Jayamani, E, Hamdan, S., Rezaur Rahman, M., Kok Heng, S., and Khusairy Bin Bakri, M (2014) Processing and Characterization of Epoxy/Luffa Composites: Investigation on Chemical Treatment of Fibers on Mechanical and Acoustical Properties, "Acoustic absorbers," BioResources 9(3), 5542-5556.

Kase, E.W. (1970) *A Study of the Role of Krisa in the Mycenaean Era,* MA thesis in the Loyola University, Chicago.

Kačuráková, M., Wilson, R.H., (2001). Developments in mid-infrared FT-IR spectroscopy of selected carbohydrates. *Carbohydr. Polym*. 44, 291–303. https://doi.org/10.1016/S0144-8617(00)00245-9

Koh.A.J., Birney.K.J, Roy.I.M, Liritzis.I (2020) The Mycenaean citadel and environs of Desfina-Kastrouli: a transdisciplinary approach to southern Phokis, *Mediterranean Archaeology and Archaeometry,* Vol. 20, No 3, (2020), pp. 47-73. DOI: 10.5281/zenodo.3930420.

Kontopoulos, I., Penkman, K., Liritzis, I., Collins, M.J (2019) Bone diagenesis in a Mycenaean secondary burial (Kastrouli, Greece). Archaeol Anthropol Sci 11, 5213–5230. https://doi.org/10.1007/s12520-019-00853-0.

Knodell, A (2021). Societies in Transition in Early Greece: An Archaeological History, University of California Press, Oakland, Table 1, p. 7.

Kubovský, I., Kačíková, D. and Kačík, F. (2020) Structural changes of oak wood main components caused by thermal modification, *Polymers,* 12(2). doi: 10.3390/polym12020485.

Lewis, S.P., Lewis, A.T., Lewis, P.D., (2013). Prediction of glycoprotein secondary structure using ATR-FTIR. *Vib. Spectrosc*. 69, 21–29. https://doi.org/10.1016/j.vibspec.2013.09.001

Liang, C.Y., Marchessault, R.H., (1959). Infrared spectra of crystalline polysaccharides. I. Hydrogen bonds in native celluloses. *J. Polym. Sci*. 37, 385–395. https://doi.org/10.1002/pol.1959.1203713209

Levy,T.E, T. Sideris, M. Howland, B. Liss, G. Tsokas, A. Stambolidis, E. Fikos, G. Vargemezis, P. Tsourlos, A. Georgopoulos, G. Papatheodorou, M. Garaga, D. Christodoulou, R. Norris, I. Rivera-Collazo, and I. Liritzis (2018) At-Risk World Heritage, Cyber, and Marine Archaeology: The Kastrouli–Antikyra Bay Land and Sea Project, Phokis, Greece , Springer International Publishing AG In T.E. Levy, I.W.N. Jones (eds.), *Cyber-Archaeology and Grand Narratives, One World Archaeology*, 143-230 (doi-org-443.webvpn.fjmu.edu.cn/10.1007/978-3-319-65693-9_9)

Lazaridis, I., Alpaslan-Roodenberg, S., et al., (2022) The genetic history of the Southern Arc: A bridge between West Asia and Europe. *Science* 377, 939.

Liritzis, I.; Polymeris, G.S.; Vafiadou, A.; Sideris, A.; Levy, T.E. Luminescence dating of stone wall, tomb and ceramics of Kastrouli (Phokis, Greece) Late Helladic settlement: Case study. *J. Cult. Herit*. 2018, 35, 76–85.

Liritzis, I (2021) Kastrouli fortified settlement (Desfina, Phokis, Greece): a chronicle of research. *SCIENTIFIC CULTURE*, Vol. 7, No. 2, pp. 17-32. DOI: 10.5281/zenodo.4465472

Liritzis, I, Xanthopoulou, V, Palamara, E, Papageorgiou, I, Iliopoulos, I, Zacharias, N, Vafiadou, A, Karydas A.G. (2020) Characterization and provenance of ceramic artifacts and local clays from late Mycenaean Kastrouli (Greece) by means of P-XRF screening and statistical analysis. *Journal of Cultural Heritage*, 46, 61–81.

Liritzis, I., Jin, Z., Fan, A., Sideris, A., Drivaliari, A., (2016) Later Helladic and later reuse phases of Kastrouli settlement (Greece); preliminary dating results. *Mediterranean Archaeology and Archaeometry* 16(3), 245-250.

Liritzis, I (2022) The ancient DNA of the N.E. Mediterranean/Euro-Asian Cultures and the Position of the Mycenaean Greeks among the first Cultures*, Proceedings of the European Academy of Sciences & Arts,* Vol.1, No 1, 7-14. https://www.peasa.eu/ancient-dna-of-the-mediterranean-euro-asian-cultures/; DOI: 10.5281/zenodo.7031096.

Marques, M.P.M., Mamede, A.P., Vassalo, A.R., Makhoul, C., Cunha, E., Gonçalves, D., Parker, S.F., Batista de Carvalho, L.A.E., 2018. Heat-induced Bone Diagenesis Probed by Vibrational Spectroscopy. *Sci. Rep*. 8, 1–13. https://doi.org/10.1038/s41598-018-34376-w.

Maniatis, Y (2013) The Radiocarbon method for dating of archaeological and environmental materials, in D. Grammenos (ed.), Research on prehistoric Macedonia, e-journal Proistorimata, Suppl. 1 (in Greek), available on http://proistoria.wordpress.com

Maniatis, Y., Ch. Oberlin, Z. Tsirtsoni, (2016) 'BALKANS 4000': The Radiocarbon dates from archaeological contexts. In: Tsirtsoni Z, editor. The human face of radiocarbon, TMO 69, Maison de l'Orient et de la Méditerranée. Lyon, pp. 41-65.

Mamede, A.P., Gonçalves, D., Marques, M.P.M., Batista de Carvalho, L.A.E., 2018. Burned bones tell their own stories: A review of methodological approaches to assess heat-induced diagenesis. Appl. Spectrosc. Rev. 53, 603–635. https://doi.org/10.1080/05704928.2017.1400442

Mastrokostas, E. (1956) Prehistoric settlements in Western Locris, Phokis and Boeotia (Προϊστορικοί συνοικισμοί εν Εσπερία Λοκρίδι, Φωκίδι και Βοιωτία), *Arkheologiki Ephimeris*, pp. 22-22 (in Greek).

Mountjoy, P (1998) The East Aegean-West Anatolian Interface in the Late Bronze Age: Mycenaeans and the Kingdom of Ahhiyawa. *Anatolian Studies* 48, 33-67.

Mohamed, I., Osman, A., Wahdan, K., Sitohy, M., (2019). Chemical Evaluation and Functional Properties of Luffa Seeds Protein. *Zagazig J. Agric. Res*. 46, 467–474. https://doi.org/10.21608/zjar.2019.33401

Nielsen-Marsh, C.M., Hedges, R.E.., 2000. Patterns of Diagenesis in Bone I: The Effects of Site Environments. J. Archaeol. Sci. 27, 1139–1150. https://doi.org/10.1006/jasc.1999.0537.

Philippson, A. & Kirsten, E. (1951) *Das Östliche Mittelgriechenland und die Insel Euboea. Die Griechischen Landschaften*, vol. I, part II, Frankfurt am Main.

Pournou, A. (2020) *Biodeterioration of Wooden Cultural Heritage*. Cham: Springer International Publishing. doi: 10.1007/978-3-030-46504-9.

Polymeris, G.S., Liritzis, I., Levy, T.E (2023) Radiocarbon dating of Kastrouli settlement: A Critical assessment. *Journal of Cultural Heritage* (in press).

Poliszuk, A., Ybarra, G., (2014). Analysis of cultural heritage materials by infrared spectroscopy, in: Cozzolino, D. (Ed.), *Infrared Spectroscopy: Theory, Developments and Applications.* Nova Science Publishers, New York, pp. 519–536.

Rice, M., (1987). *Pottery analysis*. Chicago: University of Chicago Press.

Rye, O. S., (1981). *Pottery technology: principles and reconstruction*. Washington D. C.: Taraxacum.

Reimer P, Austin W, Bard E, Bayliss A, Blackwell P, Bronk Ramsey C, Butzin M, Cheng H, Edwards R, Friedrich M, Grootes P, Guilderson T, Hajdas I, Heaton T, Hogg A, Hughen K, Kromer B, Manning S, Muscheler R, Palmer J, Pearson C, van der Plicht J, Reimer R, Richards D, Scott E, Southon J, Turney C, Wacker L, Adolphi F, Büntgen U, Capano M, Fahrni S, Fogtmann-Schulz A, Friedrich R, Köhler P, Kudsk S, Miyake F, Olsen J, Reinig F, Sakamoto M, Sookdeo A, Talamo S. (2020). The IntCal20 Northern Hemisphere radiocarbon age calibration curve (0–55 cal kBP). *Radiocarbon* 62(4): 725–757.

Stuiver, M and Polack, H.A (1997) Discussion reporting of 14C data, *Radiocarbon* 19, pp. 355–363

Sideris, A. (2014) *Antikyra. History and Archaeology,* Athens (in Greek).

Sideris, A (2022) The Mycenaean site of Kastrouli, Phokis, Greece: third excavation season, July 2018. Mediterranean Archaeology and Archaeometry, Vol. 22, No 2, 1-21.

Sideris, A and Liritzis, I (2018) The Mycenaean site of Kastrouli, Phokis, Greece: second excavation season, July 2017. *Mediterranean Archaeology and Archaeometry*, Vol. 18, No 3, 209-224.

Sideris, A, Liritzis, I, Liss, B, Howland, M.D, Levy, T.E (2017) At-risk cultural heritage: New excavations and finds from the Mycenaean site of Kastrouli, Phokis, Greece, *Mediterr. Archaeol. Archaeom*. 17 (1), 271–285.

Skals, I., Gleba, M., Taube, M & Mannering, U (2018) Wool textiles and archaeometry: testing reliability of archaeological wool fibre diameter measurements. *Danish Journal of Archaeology,* 7:2, 161-179, DOI: 10.1080/21662282.2018.1495917.

Steele, D., (2006). Infrared Spectroscopy: Theory, in: Chalmers, J.M. (Ed.), *Handbook of Vibrational Spectroscopy.* John Wiley & Sons, Ltd, Chichester, UK. https://doi.org/10.1002/0470027320.s0103.

Tartaron, T. F. (2013) Maritime networks in the Mycenaean world, Cambridge - New York

Thallemer, A (2020) Sponges versus foams: Nature and human artefact THE GLOBAL LIFE OF SPONGES, Emery, E (ed), Proceedings of the International Sponges Conference [SOAS, University of London], Island of Hydra, Greece, 19-20 May 2018, RN Books, pp. 29-36

Trueman, C.N.G., Behrensmeyer, A.K., Tuross, N., Weiner, S. (2004) Mineralogical and compositional changes in bones exposed on soil surfaces in Amboseli National Park, Kenya: diagenetic mechanisms and the role of sediment pore fluids, J. Archaeol. Sci, 31, 721-739.

Voultsiadou, E (2007) Sponges: an historical survey of their knowledge in Greek antiquity, *J. Mar. Biol. Ass.* U.K. (2007), 87, 1757–1763.

Vitale, S (2006) The LH IIIB – LH IIIC Transition on the Mycenaean Mainland. Ceramic Phases and Terminology, *Hesperia* 75: 177–204.

Vasko, P. D., Blackwell, J. and Koenig, J. L. (1971) Infrared and raman spectroscopy of carbohydrates. Part I: Identification of OH and CH-related vibrational modes for D-glucose, maltose, cellobiose, and dextran by deuterium-substitution methods, *Carbohydrate Research*, 19(3), pp. 297–310. doi: 10.1016/S0008-6215(00)86160-1.

Vasko, P. D., Blackwell, J. and Koenig, J. L. (1972) Infrared and raman spectroscopy of carbohydrates: Part II: Normal coordinate analysis of α-D-glucose, *Carbohydrate Research,* 23(3), pp. 407–416. doi: 10.1016/S0008-6215(00)82690-7.

Wiercigroch, E., Szafraniec, E., Czamara, K., Pacia, M.Z., Majzner, K., Kochan, K., Kaczor, A., Baranska, M., Malek, K., (2017). Raman and infrared spectroscopy of carbohydrates: A review. *Spectrochim. Acta Part A Mol. Biomol. Spectrosc*. 185, 317–335.

Weiner, S., (2010). *Microarchaeology,* 1st ed. Cambridge University Press, Cambridge. https://doi.org/10.1017/CBO9780511811210

Wiener, M. (2003). The absolute chronology of Late Helladic III A2 revisited. The *Annual of the British School at Athens*, 98, 239-250.

Weiner, S., Bar-Yosef, O., 1990. States of preservation of bones from prehistoric sites in the Near East: A survey. J. Archaeol. Sci. 17, 187–196. https://doi.org/10.1016/0305-4403(90)90058-D

Warren, F. J., Gidley, M. J. and Flanagan, B. M. (2016) Infrared spectroscopy as a tool to characterise starch ordered structure - A joint FTIR-ATR, NMR, XRD and DSC study, *Carbohydrate Polymers,* 139, pp. 35–42. doi: 10.1016/j.carbpol.2015.11.066.

Wiercigroch, E. et al. (2017) Raman and infrared spectroscopy of carbohydrates: A review, *Spectrochimica Acta Part A: Molecular and Biomolecular Spectroscopy,* 185, pp. 317–335. Available at: http://dx.doi.org/10.1016/j.saa.2017.05.045.